

**ROUND WIRES VERSUS TRAPEZOIDAL WIRES IN
ACSR AND ACSS OVERHEAD POWER TRANSMISSION
CONDUCTORS**

by

LUNGILE PEGGY LUHLANGA

(Student Number: 212561623)

Submitted in fulfilment of the academic requirements for the degree of Master of Science in
Electrical Engineering

School of Engineering,

Discipline of Electrical Engineering,

Supervisor: **Dr Akshay Saha**

Co-supervisor: **Dr Rob Stephen**

University of KwaZulu-Natal Durban

February 2015

As the candidate's supervisor I have approved this thesis/dissertation for submission.

Signed:

Name: **Dr Akshay Saha (Supervisor)**

Date: February 2015

ABSTRACT

In overhead power transmission, the greatest need is to transmit maximum power with reduced losses, minor environmental impact and minimal infrastructure degradation, at low costs. The conductor material and shape (form) are deemed to be amongst the main determinants for optimal power transfer. Various forms such as trapezoidal (TW), aero-z (Z) and round-wires (RW) have been developed for bare overhead power transmission conductors. About 80 % of power utilities around the globe, including South Africa, use Aluminium Conductor Steel reinforced (ACSR) conductors formed in RW for power transmission lines at voltages above 132 kV. Interest is also shown by some power utilities to use High Temperature Low Sag (HTLS) conductors, mostly Aluminium Conductor Steel Supported (ACSS) for short transmission lines. In this study electrical performances of ACSR and ACSS conductors in TW and RW forms were evaluated. The electrical characteristics considered are thermal ratings, power losses and magnetic fields. Particular reference was made to Eskom's 400 kV power line, using the Power Line Systems - Computer Aided Design and Drafting (PLS-CADD) software program for the magnetic fields analysis. RateKit 5.0 software which uses both IEEE 738-2002 (IEEE) and CIGRÉ methods was used for conductor thermal rating calculations. The power losses were calculated using the resistances and the maximum allowable current on the conductor. The results showed slight differences between RW and TW in terms of the electrical performances. Most of the differences are due to the variances in resistances and diameters of the conductors resulting from the shape of the conductor.

DECLARATION 1 – PLAGIARISM

I, Lungile Peggy Luhlanga, declare that

1. The research reported in this thesis, except where otherwise indicated, is my original research.
2. This thesis has not been submitted for any degree or examination at any other university.
3. This thesis does not contain other persons' data, pictures, graphs or other information, unless specifically acknowledged as being sourced from other persons.
4. This thesis does not contain other persons' writing, unless specifically acknowledged as being sourced from other researchers. Where other written sources have been quoted, then:
 - a. Their words have been re-written but the general information attributed to them has been referenced
 - b. Where their exact words have been used, then their writing has been placed in italics and inside quotation marks, and referenced.
5. This thesis does not contain text, graphics or tables copied and pasted from the Internet, unless specifically acknowledged, and the source being detailed in the thesis and in the References sections.

Signed:

.....

DECLARATION 2 - PUBLICATIONS

DETAILS OF CONTRIBUTION TO PUBLICATIONS that form part and/or include research presented in this thesis (include publications in preparation, submitted, *in press* and published and give details of the contributions of each author to the experimental work and writing of each publication)

Publication 1

LP. Luhlanga, AK. Saha, Review of bare conductors for overhead power transmission, SAUPEC 2013, Potchefstroom University, 31 January – 01 February 2013.

Publication 2

LP. Luhlanga, AK. Saha, RG. Stephen, Comparisons of conductor thermal rating models for high temperature operations, First Eskom Power Plant Engineering Institute Student Conference Eskom Academy of Learning, 5 & 6 May 2014.

Signed:

.....

ACKNOWLEDGEMENT

I would like to express my appreciation to the Eskom Power Plant Engineering Institute (EPPEI) for granting me the opportunity and the funds to complete my studies. I thank my academic and industrial supervisors; Dr. Saha and Dr. Rob Stephen for their dedication and guidance throughout the duration of the project. I express my sincere thankfulness to my manager, Riaz Vajeth, for the two-year out-of-work permission to complete the work. My colleagues, Rishen Moodely, Lebo Maphumulo, Tebogo Bhulose and Ndangi Muthadi are highly acknowledged for their contributions on the project especially the PLS-CADD program. I also would like to thank Professor Dzevad Muftic for providing relevant information for the project. Mr. Stefaan Greyling and Mr. Suvir Maharaj at Trans-Africa Projects are highly acknowledged for providing a crèche course for PLS-CADD. A lot of appreciation goes to Thomas from Southwire®, for providing the PLS-CADD conductor files. Benjamin from Nexans® is thanked for the information on the use of the RateKit program and its supporting documentation. Dr. Dale Douglas is appreciated for the verification of the thermal rating results.

Lastly, I would like to appreciate the Holy Spirit for the strength, encouragement, tenacity and the ability He granted to ensure completion of the work in time. All glory belongs to the Living God!

LP Luhlanga

Table of Contents

ABSTRACT II

DECLARATION 1 – PLAGIARISM.....III

DECLARATION 2 - PUBLICATIONS.....IV

ACKNOWLEDGEMENTV

DEFINITIONS AND ABBREVIATIONS:..... 1

LIST OF FIGURES 3

LIST OF TABLES 5

LIST OF SYMBOLS 6

CHAPTER 1 9

INTRODUCTION..... 9

1.1 PROBLEM DEFINITION..... 9

1.2 BACKGROUND 9

1.2.1. MINIMUM ELECTRICAL CLEARANCES..... 10

1.2.2. MAGNETIC FIELDS..... 11

1.2.3. CONDUCTOR PHYSICAL PROPERTIES 11

1.2.4. ACSR VERSUS ACSS CONDUCTORS 12

1.2.5. TW VERSUS RW 12

1.2.6. ELECTRICAL POWER LOSSES..... 13

1.3 RESEARCH QUESTION 14

1.4 PROJECT AIMS AND OBJECTIVES 15

1.5 STRUCTURE OF THESIS..... 15

CHAPTER 2	17
LITERATURE REVIEW	17
2.1 INTRODUCTION	17
2.2 HISTORY OF CONDUCTOR THERMAL RATINGS	17
2.3 THERMAL RATING MODELS	18
2.4 IEEE AND CIGRÉ MODELS	18
2.4.1. HEAT BALANCE EQUATION	18
2.4.2. CONDUCTOR CURRENT HEATING.....	19
2.4.3. SOLAR HEAT GAIN	21
2.4.4. CONVECTION HEAT LOSS	22
2.4.5. RADIATIVE HEAT LOSS	25
2.4.6. THERMAL RATINGS CALCULATIONS	25
2.5 METEOROLOGICAL INFORMATION FOR STEADY STATE THERMAL RATING	25
2.6 PREVIOUS ELECTRICAL STUDIES ON RW AND TW CONDUCTORS	26
2.7 CONCLUSION	27
CHAPTER 3	29
METHODOLOGY	29
3.1 BACKGROUND	29
3.2 RATEKIT	30
3.3 METHOD FOR CALCULATING MAGNETIC FIELDS	34
3.3.1. TRANSMISSION LINE PARAMETERS.....	35
3.3.1. STRUCTURES FOR APOLLO - VERWOERDBURG LINE	36
3.3.2. CONDUCTOR DATA USED IN PLS-CADD	37
3.4 CONCLUSION	38
CHAPTER 4	39

ELECTRICAL ANALYSIS OF TW AND RW	39
4.1 INTRODUCTION.....	39
4.2 CIGRÉ VERSUS IEEE IN AMPACITY CALCULATIONS	39
4.3 EFFECT OF TEMPERATURE ON RESISTANCE	47
4.4 TW AND RW AMPACITY COMPARISONS	49
4.5 POWER LOSSES COMPARISONS.....	51
4.6 MAGNETIC FIELD RESULTS	54
4.7 SUMMARY	58
<u>CHAPTER 5</u>	<u>59</u>
CONCLUSIONS AND RECOMMENDATIONS	59
<u>REFERENCES.....</u>	<u>62</u>
<u>APPENDICES.....</u>	<u>69</u>
APPENDIX A	69
APPENDIX B.....	77
APPENDIX C	82

DEFINITIONS AND ABBREVIATIONS:

AAC	All Aluminium Conductor
ACSR	Aluminium Conductor Steel Reinforced.
ACSS	Aluminium Conductor Steel Supported.
Ampacity	The maximum electrical current on a conductor, required for conductor sag resulting in safe electrical clearance on a transmission line.
Annealing	The process whereby the tensile strength of a material is reduced at sustained high temperatures to improve its conductivity and to prevent inelastic elongation.
ASTM	American Society for Testing and Materials.
Clearance	Distance between the conductor and the ground or nearest object
COE	The Coefficient of Linear Expansion, which is the rate at which a conductor expands in length as temperature increases.
Creep	Permanent elongation of a material due to loads that are lower than the material's yield strength
Electrical Clearance	The distance between energized conductors and other conductors, buildings, and ground.
Final Sag	The sag after elongation from creep and loading events
I.A.C.S. or IACS	International Annealed Copper Standard.
ICNIRP	International Commission on Non-Ionizing Radiation Protection
IEC	International Electrotechnical Commission.
IEEE	The Institute of Electrical and Electronics Engineers.

Definitions and Abbreviations

Initial Sag	The sag when the conductor is first installed without electrical loading on it.
Knee-point Temperature	The conductor temperature above which the aluminium strands of an ACSR or ACSS conductor have no tension but compression.
Sag temperature	The conductor temperature (with no wind nor ice) at which the sag tension (or catenary) is specified.
Sag	Distance which the conductor departs from a straight line.
Stranded Conductor	A conductor made by twisting together a group of wires.
Templating Temperature	Maximum temperature at which a conductor can safely operate without violating electrical clearances.
WHO	World Health Organization

LIST OF FIGURES

FIGURE 1-1: FACTORS AFFECTING THE SAG CHARACTERISTICS OF CONDUCTORS [5] 10

FIGURE 1-2: RW-WIRE AND TW CONDUCTOR CONFIGURATIONS [16] 13

FIGURE 1-3: VARIATION OF TRANSMISSION LOSS AND THE CORRESPONDING COST OF
 CONDUCTOR FOR A 1000 KM LINE [23]. 14

FIGURE 2-1: HEAT GAINED AND LOST THROUGH AN OVERHEAD POWER LINE CONDUCTOR 19

FIGURE 3-1: TERN AND MARTIN RW CONDUCTOR STRANDING [40]..... 29

FIGURE 3-2: THERMAL RATING CALCULATION OVERVIEW IN RATEKIT [5] [29] [45] 30

FIGURE 3-3: GOOGLE EARTH MAP SHOWING THE LINE ROUTE FOR APOLLO-VERWOERDBURG
 400 kV LINE 36

FIGURE 3-4: EXAMPLE OF SUSPENSION AND DEAD-END STRUCTURES [62]..... 36

FIGURE 4-1: IEEE AND CIGRÉ MODELS COMPARISON WITH TERN ACSR CONDUCTOR IN RW
 SHAPE 40

FIGURE 4-2: IEEE AND CIGRÉ MODELS COMPARISON WITH TERN ACSR CONDUCTOR IN TW
 SHAPE 41

FIGURE 4-3: IEEE AND CIGRÉ MODELS COMPARISON WITH TERN ACSS CONDUCTOR IN RW
 SHAPE 41

FIGURE 4-4: IEEE AND CIGRÉ MODELS COMPARISON WITH TERN ACSS CONDUCTOR IN TW
 SHAPE 42

FIGURE 4-5: IEEE AND CIGRÉ MODELS COMPARISON WITH MARTIN ACSR CONDUCTOR IN RW
 SHAPE 43

FIGURE 4-6: IEEE AND CIGRÉ MODELS COMPARISON WITH MARTIN ACSR CONDUCTOR IN TW
 SHAPE 43

FIGURE 4-7: IEEE AND CIGRÉ MODELS COMPARISON WITH MARTIN ACSS CONDUCTOR IN RW
 SHAPE 44

FIGURE 4-8: IEEE AND CIGRÉ MODELS COMPARISON WITH MARTIN ACSS CONDUCTOR IN TW
 SHAPE 44

FIGURE 4-9: AMPACITY DIFFERENCE PERCENTAGES OF THERMAL MODELS WITH ACSR
 CONDUCTOR 45

FIGURE 4-10: AMPACITY DIFFERENCE PERCENTAGES OF THERMAL MODELS WITH ACSS
 CONDUCTOR 45

FIGURE 4-11: ACSR TW AND RW CONDUCTORS’ RESISTANCE TO TEMPERATURE
 RELATIONSHIPS 48

FIGURE 4-12: ACSS TW AND RW CONDUCTORS’ RESISTANCE TO TEMPERATURE
 RELATIONSHIPS 48

List of Figures

FIGURE 4-13: AMPACITY PLOTS OF ACSR CONDUCTORS IN TW AND RW FORMS OF DIFFERENT DIAMETERS	50
FIGURE 4-14: AMPACITY PLOTS OF ACSS CONDUCTORS IN TW AND RW FORMS OF DIFFERENT DIAMETERS	50
FIGURE 4-15: AMPACITY PLOTS OF ACSR AND ACSS CONDUCTORS IN RW FORMS.....	51
FIGURE 4-16: POWER LOSSES COMPARISONS OF ACSR CONDUCTORS IN TW AND RW SHAPES	52
FIGURE 4-17: POWER LOSSES COMPARISONS OF ACSS CONDUCTORS IN TW AND RW SHAPES	53
FIGURE 4-18: ACSR MAGNETIC FIELDS AT CONDUCTOR TEMPERATURE OF 100 °C	56
FIGURE 4-19: ACSR MAGNETIC FIELDS AT CONDUCTOR TEMPERATURE OF 120 °C	56
FIGURE 4-20: ACSS MAGNETIC FIELDS AT CONDUCTOR TEMPERATURE OF 250 °C.....	57
FIGURE 4-21: ACSS MAGNETIC FIELDS AT CONDUCTOR TEMPERATURE OF 250 °C.....	58

LIST OF TABLES

TABLE 1-1: MAGNETIC FIELDS LIMITS SPECIFIED BY ICNIR [12]	11
TABLE 2-1: SOLAR AZIMUTH CONSTANT, C, AS A FUNCTION OF HOUR ANGLE, Ω , AND SOLAR AZIMUTH VARIABLE	22
TABLE 3-1: TERN AND MARTIN CONDUCTOR PARAMETERS [20] [40] [55].....	31
TABLE 3-2: APOLLO-VERWOERDBURG 400 kV LINE DESIGN PARAMETERS.....	35
TABLE 3-3: STRUCTURE INFORMATION USED IN PLS-CADD.....	37
TABLE 4-1: METEOROLOGICAL INPUT ASSUMPTIONS [45] [65].....	39
TABLE 4-2: HEAT ENERGY COMPONENTS WITH TERN ACSR RW CONDUCTOR AT $T_c = 70^\circ\text{C}$..	46
TABLE 4-3: HEAT ENERGY COMPONENTS WITH MARTIN ACSR RW CONDUCTOR AT $T_c = 70^\circ\text{C}$	46
TABLE 4-4: HEAT ENERGY COMPONENTS WITH TERN ACSS RW CONDUCTOR AT $T_c = 150^\circ\text{C}$.	46
TABLE 4-5: HEAT ENERGY COMPONENTS WITH MARTIN ACSS RW CONDUCTOR AT $T_c = 150^\circ\text{C}$	47
TABLE 4-6: PERCENTAGE DIFFERENCES BETWEEN RW AND TW CONDUCTORS OF ACSR TYPES	52
TABLE 4-7: PERCENTAGE DIFFERENCES BETWEEN RW AND TW CONDUCTORS OF ACSS TYPES	53
TABLE 4-8: AMPACITY VALUES USED FOR MAGNETIC FIELD CALCULATIONS OF ACSR CONDUCTORS	55
TABLE 4-9: AMPACITY VALUES USED FOR MAGNETIC FIELD CALCULATIONS OF ACSS CONDUCTORS	57
TABLE C-1: AMPACITY OF IEEE AND CIGRÉ FOR MARTIN ACSR CONDUCTOR IN TW SHAPE	82
TABLE C-2: AMPACITY OF IEEE AND CIGRÉ FOR MARTIN ACSR CONDUCTOR IN RW SHAPE	83
TABLE C-3: AMPACITY OF IEEE AND CIGRÉ FOR TERN ACSR CONDUCTOR IN RW	84
TABLE C-4: AMPACITY OF IEEE AND CIGRÉ FOR TERN ACSR CONDUCTOR IN TW	85

LIST OF SYMBOLS

Symbol	Explanation	Units
I	Conductor current	A
I_{rating}	Maximum allowable current on the conductor	A
$R(T_c)$	Conductor resistance at a given temperature	Ω/km
T_a	Ambient temperature	$^{\circ}\text{C}$
T_o	Initial conductor temperature	$^{\circ}\text{C}$
T_c	Conductor temperature	$^{\circ}\text{C}$
T_{High}	Higher value of temperature at which conductor resistance is calculated.	$^{\circ}\text{C}$
T_{Low}	Lower value of temperature at which conductor resistance is calculated.	$^{\circ}\text{C}$
T_f	Average conductor surface temperature	$^{\circ}\text{C}$
Q_{cn}	Convective cooling based on the IEEE method	W/m
Q_{c1}	IEEE convective cooling at low wind speeds	W/m
Q_{c2}	IEEE convective cooling at high wind speeds	W/m
Q_r	Heat lost by the conductor due to radiation	W/m
Q_s	Conductor heat gained due to solar radiation	W/m
Q_w	Evaporative cooling	W/m
Q_c	Convective cooling based on CIGRÉ method	W/m
Q_j	Joule heating	W/m
Q_m	Magnetic heating	W/m
Q_i	Corona heating	W/m
Q_w	Evaporative cooling	W/m

List of Symbols

Symbol	Explanation	Units
k_f	Thermal conductivity of air	W/(m [·] °C)
I_{dc}	DC current	A
I_{ac}	AC current	A
R_{dc}	Conductor DC resistance	Ω/km
R_{ac}	Conductor AC resistance	Ω/km
α	Conductor temperature coefficient	K ⁻¹
k_j	Skin effect factor	dimensionless
ϵ	Emissivity of conductor material	dimensionless
a	Absorptivity of conductor surface	dimensionless
D	External conductor diameter	m
S	Global solar radiation	dimensionless
θ	Effective angle of incidence of the sun's rays	degrees
k_{angle}	Wind direction factor	dimensionless
μ_f	Thermal conductivity of air	°C
V_w	Wind velocity	m/s
ρ_f	Air density	Kg/m ³
H_e	Elevation of conductor above sea level	m
SAG	Conductor sag	m
d_s	Bundle diameter	mm
H	Magnetic flux density	A/m
B	Magnetic field	T
μ	Permeability of a material	H/m

List of Symbols

Symbol	Explanation	Units
I_r	Real current component	A
I_i	Imaginary component of current	A

Chapter 1

INTRODUCTION

1.1 Problem Definition

Electricity utilities around the globe in developed and developing countries are faced with an increasing avalanche of power consumption [1] [2]. Tied with the enormous consumption is the difficulty to acquire right of way for new transmission line constructions because of escalating cost of land; and environmental impact associated with transmission lines [1] [2] [3] [4]. The construction of new power lines has become more challenging [4]. Hence, transmission line designers are forced to find safe alternatives to improve the power transfer capabilities of both new and existing lines at low costs [2] [3].

Reduction of power losses, minimizing environmental impact, increasing the conductor current carrying capacity and reducing infrastructure degradation are among the available alternatives to maximize power transfer [1] [2] [4]. These alternatives are directly linked with the choice of conductor used on the transmission line. Conductor manufactures have configured bare conductors in special forms or shapes and have developed diverse material compositions to improve the conductor properties for maximum power transfer capabilities [5].

Available conductor forms comprise trapezoidal wires, aero-z wires and round-wires [6]. Conductor materials such as invar, gap-type, and fully annealed aluminium, composite and metal matrix have been developed for operations at high temperatures – so called high temperature low sag conductors (HTLS) [4] [5]. The use of HTLS conductors in overhead power transmission was introduced in the late 70's as a solution to improve power transfer capabilities of transmission lines [7] [5]. The electrical behaviour comparisons of the shaped conductors and the new material compositions (HTLS) with conventional conductors are vitally important to determine whether these conductors can indeed offer improved power transfer benefits [5]. For this reason, this study aims to evaluate and contrast the current carrying capacities of ACSR and ACSS in round and trapezoidal forms and to determine their maximum allowable conductor temperatures. Magnetic fields evaluation was done to ascertain that the conductors emit magnetic fields within the statutory limits when operated at high temperatures. Power losses comparisons were computed for the TW and RW conductors.

1.2 Background

The transfer of electrical energy from generating power stations to substations near the load centers is achieved through high voltage transmission lines. In South Africa, transmission lines

at voltages of 132 kV and above utilize overhead bare conductors. Bare conductors are exposed to numerous hitches which encompass enormous electrical power losses, wire damages caused by vibration, corrosion, increased thermal operation of conductors and severe weather conditions such as, varying temperature, rain, wind and ice loading [1] [8].

The current carrying capacity of a conductor is principally militated by its thermal limits [1]. Thermal exposure results in conductor permanent elongation and loss of strength [8] [9]. Hence, the basis for a transmission line rating is the ability of the designed line to maintain safe clearance between energized conductors and the ground objects directly below the line and to ensure that the maximum operating temperature of the conductor is not exceeded [9]. Electrical ground clearances have a direct impact on public safety, such as magnetic field exposure and electrocution and it is a function of the conductor physical properties.

1.2.1. Minimum Electrical Clearances

Transmission lines are designed to conform to the electrical clearances recommended by statutory laws [10] [11]. The sag curve shown in Figure 1-1 illustrates the effects of conductor sag, due to the conductor material elongation, from various factors, on the minimum required conductor to ground clearance [5]. Apart from thermal elongation, a transmission line sags due to the conductor weight, ultimate tension, and high wind or ice loading, as illustrated in Figure 1-1 [5]. The maximum or final sag is calculated so that clearance to ground and to other conductors is maintained at the different loading conditions.

The final sag, resulting from operating the conductor at its maximum temperatures, determines the minimum electrical clearance to ground and conductor blowout to minimize electromagnetic field exposure to the public in the vicinity of the power line [5].

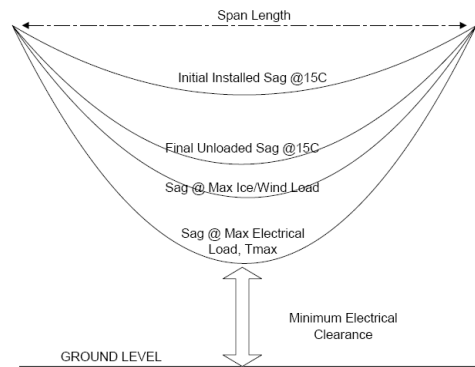


Figure 1-1: Factors affecting the sag characteristics of conductors [5]

1.2.2. Magnetic Fields

Power frequency magnetic fields generated by overhead power lines have been of interest since the 1970's because of public concerns that they might affect biological systems [12] [13]. Moreover, the magnetic fields are said to impose short term internal body currents on live line workers [14] [15]. The induced currents result in nauseating micro-shocks on the live line workers [14] [15]. Although research efforts have failed to find a link between electromagnetic fields and any harmful effect on human beings, the concerns on public safety against magnetic fields is increasing [13]. For this reason WHO and ICNIRP imposed limits associated with magnetic fields emissions within the frequency range of a transmission line, presented in Table 1-1 [12]. Electromagnetic fields at power frequency are quasi-static, thus the magnetic fields are assumed to be generated by the current on the conductor only [15]. An increase in the conductor current increases the magnetic fields within the right of way and in the vicinity of the transmission line [15]. Hence, it is required that whenever the current carrying capacities of conductors are calculated, the magnetic field quantities are verified if they are within the stipulated limits. Since the thermal ratings of the conductors of RW and TW are compared, also the magnetic fields from these conductors will be compared.

Table 1-1: Magnetic Fields Limits Specified by ICNIR [12]

ICNIRP Magnetic Field Limits (μT)	
At Servitude Boundary	Within Servitude
100	500

1.2.3. Conductor Physical Properties

Since the conductor is one of the major components of a transmission line, it is important to understand its characteristics, to appreciate the limiting factors to the power transfer capability. The desirable conductor properties to achieve maximum power transmission include favorable strength to weight ratio, good conductivity of conducting material with high tensile strength of core [16]. Steel strands provide mechanical reinforcement to handle higher line tensions and they reduce sag in longer span lengths, whereas, aluminium provides good conductivity [16]. The behavior of a bimetallic conductor is determined by the electrical and mechanical properties of the materials making up the conductor.

1.2.4. ACSR versus ACSS Conductors

ACSR has been a standard conductor for electrical utilities since the early 1900's [17]. It consists of either a solid or stranded standard, high, extra-high or ultra-high strength steel core surrounded by one or more layers of hard drawn 1350 H19 aluminium strands [18]. The steel core wires of ACSR may be zinc galvanized with standard weight Class A coating or heavier coatings of Class B or Class C to reduce corrosion of the steel wires. The aluminium wires of ACSR conductors were first developed in RW configurations. However, TW were developed in the 1970's [17].

ACSS conductor was developed by Reynolds Metals in 1974 [19] [20]. By then the conductor was called the steel supported aluminium conductor (SSAC) [21]. ACSS conductor resembles the ACSR in appearance, stranding and overall diameter [21]. However, ACSS uses fully annealed 1350 HO aluminium strands instead of the 1350 H19 used in standard ACSR [19]. Compared to an equal size ACSR, ACSS has more conductivity, lower breaking strength, lower creep elongation and lower elastic modulus [19]. The initial application of ACSS conductor was on long spans where the sag was very critical [18]. Nowadays the ACSS conductor is deemed to be a remedy to increase the current carrying capacity of existing lines [18].

ACSS develops most of its performance advantages from the fact that the aluminium wires are fully annealed during the manufacturing process and have very low yield strength [19] [21]. Because of the low yield strength, rapid permanent or inelastic elongation occurs in the aluminium when tension is applied to the composite conductor transferring the load to the steel core. ACSS conductors are available in RW and TW forms [19].

1.2.5. TW versus RW

Figure 1-2 shows conductor configurations in RW and TW with two layers of 30 aluminium strand, and 7 steel inner strands [16] [19] [21]. Each individual wire of a RW shaped conductor is concentrically stranded and considerable space exists between wires. Trapezoidal wires are formed by “building up” pre-shaped conductors, resulting in a very dense and flexible structure [18]. TW conductors are compacted with two available designs. One design gives an equal area of aluminium when compared to the standard RW conductor sizes. The other design gives an overall outside diameter equal to standard ACSR conductor sizes. In TW conductors all the strands can be trapezoidal in shape or only the aluminium strands can be trapezoidal [19] [21]. The TW with only the aluminium strands trapezoidal shaped, are the most common and preferred conductors.

Both the RW and TW conductors consist of a central wire or core surrounded by one or more adjacent layers of helically laid wires as illustrated in Figure 1-2 [16] [19] [21]. Each layer after the first layer has more layers than the preceding layer and is applied in a direction opposite that of the layer under it.

The use of TW designs instead of RW is founded on the bases that TW have less voids, smooth surface and a reduced outside diameter [18] [19]. TW are deemed to be free from strand “bird caging” under bending moments because of the elimination of spaces between the strands [18]. The smaller diameter, equal area TW conductors provide material reduction, which results in reduced conductor weight and prevent aeolian vibrations on the conductor because the drag coefficient is less than that of their RW counterparts. Compact weight translates to lower tension required to suspend the conductor between dead ends. Reduced weight and less tension particularly has an impact on the design strength of the support structures and hardware. Weight and tension are also linked to the mechanical sagging of the conductor. Also, with the reduced diameter in TW conductors it is expected that the effects of ice and wind loading on the conductor be reduced. Additionally, fewer voids in TW conductor prevent corrosion of steel strands [18] [19].

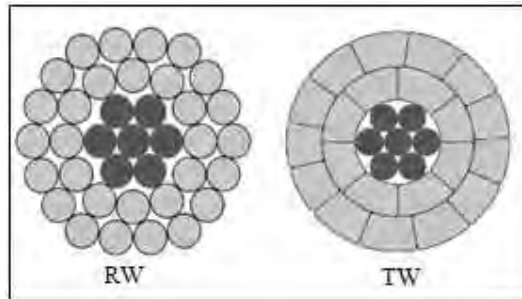


Figure 1-2: RW-Wire and TW conductor configurations [16]

1.2.6. Electrical Power Losses

Power transmission losses comprise of ohmic power losses, corona losses from the line itself and losses from other transmission network devices such as transformers, reactors, and capacitors [22]. The losses that are directly linked to the conductor are the ohmic losses and corona losses [22]. Only the ohmic losses which are due to the heat dissipation from the conductor resistance because of the current flowing through the conductor will be discussed and evaluated in this study. For a given transmission line length, the ohmic power losses are a function of the conductor resistance and the square of the electrical current [23]. The electrical resistance of a conductor is a function of conductor area and resistivity. The resistivity of the

conductor is a temperature dependent variable. The ohmic losses are expected to increase as the operating temperature or thermal rating of the conductor is increased. Moreover, power loss is one of the determinants of the cost per unit length for an overhead line and the conductor temperature attained as a result of high current levels [23] [24]. The life cycle cost of a transmission line is calculated based on the initial investment cost and the total cost of line losses [24]. The total cost of line losses includes ohmic losses.

Figure 1-3 illustrates the power losses in relation to the capital investment of the line. An optimized conductor choice falls on position M. The principle is that, a larger conductor in diameter has a reduced electrical resistance, but costs more and vice versa [23].

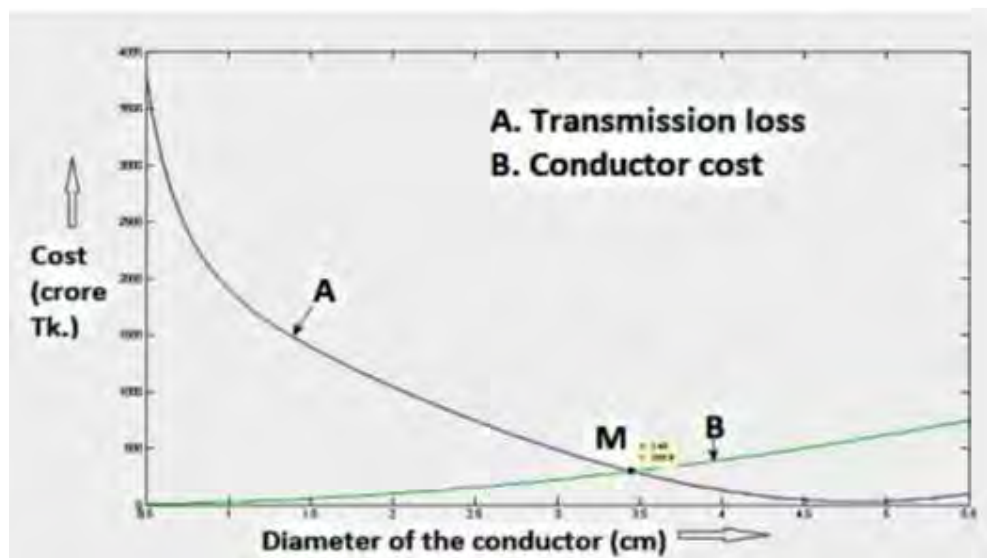


Figure 1-3: Variation of transmission loss and the corresponding cost of conductor for a 1000 km line [23].

1.3 Research Question

Although there are a number of HTLS conductor materials that have been developed, ACSS was chosen for this study because it is very similar to ACSR conductors as discussed in section 1.2. The physical similarities between ACSS and ACSR conductors make it easy to re-conductor an ACSR line with ACSS conductors. The physical and chemical properties of TW and ACSS discussed in section 1.2 entice studies to quantify the benefits that these conductors can offer especially in improving the power transfer capabilities of a transmission line when compared to their RW and ACSR counterparts.

Moreover, the reconfiguration of the conductor shape and the manipulation of the conductor materials have raised a number of questions regarding the conductor's operational behaviour as compared to the conventional designs. This research aims at answering questions such as:

- Can formed wires offer higher current carrying capacities, less magnetic fields and lower power losses when compared to RW counterparts, in addition to the known vibration and corrosion resistance advantages?

1.4 Project Aims and Objectives

The primary motivation for forging conductors into different shapes is to produce very close to smooth conductor surfaces with smaller voids in between strands to prevent corrosion, vibrations and corona losses. However, modifying the conductor's physical shape alters its diameter, conducting area and resistance. Changes in such parameters suggest some effects on the conductor current carrying capacity and power losses. Also, refining the conductor material, like in the case of HTLS conductors, aims to improve the conductor thermal ratings for increased power transfer. It is therefore of great interest to investigate and quantify the degree at which the current carrying capacity, sometimes called thermal rating, is affected by conductor forging and material modification. The factors that are closely associated with thermal ratings include the conductor sag and magnetic fields, which affect the electrical clearance to ground of transmission lines and hence public safety.

The objective of this work is to quantify the effect of material alterations and forging of conductors into different shapes on the maximum power transfer and environmental impacts using conventional models. This is done by comparing the performances of ACSR conductors to ACSS conductors referring to material alterations; and to compare TW with RW conductors with respect to conductor forging. The conductor's contribution to the maximum power transfer in this case, is to be quantified through the calculations of conductor thermal ratings, the amount of power losses and the magnetic field impact in the vicinity of a transmission line.

1.5 Structure of Thesis

This report is organized in five chapters. Chapter 1 gives an overview and background of the aim and objectives of the study. The physical properties of the conductors responsible for electrical performance are also discussed. Chapter 2 presents the literature review of the methods used for the electrical performance evaluations, motivations on why other methods were chosen over others and a summary of previous work done on similar studies. Chapter 3 illustrates the materials and the exact methods applied for the study. Chapter 4 presents the

results and the analysis of the results. Chapter 5 gives the conclusions, recommendations and future work.

Chapter 2

LITERATURE REVIEW

2.1 Introduction

It was realized in the previous chapter that there is a need to compare the electrical performances of TW with RW conductors to determine if TW conductors can offer additional benefits over RW conductors. Chapter 1 showed that there may be some differences in the electrical performances of TW and RW conductors because of their physical property differences. It was also shown in the chapter that the electrical properties of conductors that directly affect the power capabilities of the conductors comprise the ampacity, power losses, magnetic field radiations. As mentioned in the previous chapter, that industry is moving towards the application of HTLS conductors, ACSS conductors were also proposed to be studied in TW and RW.

This chapter describes the available methods used for calculating conductor thermal ratings, power losses and magnetic fields to enable the comparisons of TW and RW electrical performances. Firstly, the mathematical equations of the available thermal rating models are compared to verify their use at high temperatures. Secondly, the link between the thermal ratings of the conductors and, power losses due to the dependency of conductor resistance to temperature and the magnetic fields due to operation of conductors at maximum current is described. The criterion with which one method was chosen over another for the various calculations is discussed. Finally, a review of studies done on the subject of thermal ratings, power losses on conductors, and magnetic fields is presented.

2.2 History of Conductor Thermal Ratings

The steady-state thermal models have been progressively modified over the years, but presently the models are attributable to House and Tuttle, Webs and Morgan [25]. In a study by [26], a close correlation between the House and Tuttle with IEEE model, and Morgan with the CIGRÉ model was performed. The conclusion was that the IEEE method is comparable to House and Tuttle and the CIGRÉ model is comparable to Morgan's model.

The input variables in all of these models are the geometry of the conductor, the current or the conductor temperature, the resistance, and atmospheric variables, such as wind speed and its direction and the intensity of solar radiation [25]. If the desired output is the ampacity, the allowable conductor temperature is assumed and vice versa [27].

2.3 Thermal Rating Models

Thermal ratings in transmission lines are based on the maximum operating temperature allowed on the conductor to limit conductor damage and maintain required clearances for public safety. The IEEE and CIGRÉ standards are widely used methods of calculating the current-temperature relationship of overhead lines given the weather conditions and conductor properties, based on the heat balance equation [28] [29] [30] [31]. The equation relating electrical current to conductor temperature described in these methods can be either used to calculate the conductor temperature when the electrical current is known or to calculate the current that yields a given maximum allowable conductor temperature [27] [29]. This section aims to point out the differences observed from the equations used in the two methods.

2.4 IEEE and CIGRÉ Models

2.4.1. Heat Balance Equation

The assumptions made for thermal rating calculations are based on the fact that overhead conductors are exposed to meteorological environment [29] [30]. The calculations are affected by wind, solar radiation and ambient temperature, in addition to the electrical current on the conductors. Furthermore, steady-state condition is assumed. At steady state, the conductor heat gain is equal to the heat loss i.e. no heat energy is stored in the conductor [29] [30].

Although both the IEEE and CIGRÉ standards use the same basic heat balance concept, their approach to the calculation of the heat balance components is slightly different. Both methods agree that the heating elements are solar radiation and internal heating by the electrical current flowing through the conductor resistance or ohmic heating and that the heat loss is due to convection and radiation. However, the CIGRÉ method adds magnetic and corona heating elements and evaporative cooling to the heat balance equation. Also, the CIGRÉ method presents the heating due to current flow as magnetic and joule heating. Corona heating and evaporative cooling elements are not normally included in the actual thermal rating calculations because they cancel each other and their contribution is deemed to be insignificant [30].

The representation of the heat balance energy is indicated in Figure 2-1 and equation (2.1) [29] [30].

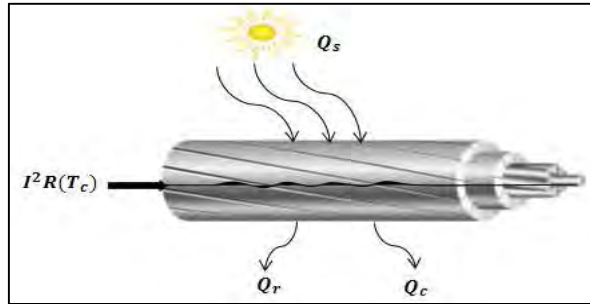


Figure 2-1: Heat gained and lost through an overhead power line conductor

According to the CIGRÉ method, the heat balance equation is represented by equation (2.1) [30].

$$Q_j + Q_m + Q_s = Q_c + Q_r \quad (2.1)$$

Q_j = Joule heating

Q_m = Magnetic heating

Q_s = Solar heating

Q_c = Convective cooling

Q_r = Radiative cooling

The IEEE method omits the magnetic heating term, and presents the heat balance equation as equation (2.2) [29].

$$Q_j + Q_s = Q_c + Q_r \quad (2.2)$$

The differences between the IEEE and the CIGRÉ are highlighted.

2.4.2. Conductor Current Heating

Current or joule heating is due to the energy generated by the current flowing through the conductor. The difference between the methods in the conductor current heating calculation is marked by the resistance calculation. The differences in the joule heating between the two methods are represented in equation (2.3) for the CIGRÉ method and in equation (2.4) for the IEEE method [29] [30].

$$Q_j = k_j I^2 R_{ac} [1 + \alpha(T_f + 20)] \quad (2.3)$$

$$Q_j = I^2 R_{ac}(T_c) \quad (2.4)$$

$$T_f = \frac{T_c + T_a}{2} \quad (2.5)$$

$$R_{ac} = k_j R_{dc} \quad (2.6)$$

k_j = skin effect factor

I = Current (A)

R_{dc} = DC resistance of conductor (Ω)

R_{ac} = AC resistance of conductor (Ω)

α = Conductor temperature coefficient

T_f = Average conductor temperature ($^{\circ}\text{C}$)

T_c = Conductor temperature ($^{\circ}\text{C}$)

T_a = Ambient temperature ($^{\circ}\text{C}$)

The AC resistance according to CIGRÉ is dependent on the DC resistance, current density in each aluminium layer of the conductor, temperature and frequency, as presented in equation (2.7). Equation (2.7) is based on the work done by [32] [33] [34] [35] [36] [37] and [38], where the AC resistance was found to be influenced by the magnetic flux density in steel-cored conductors. The constants b and m represent the increment of the resistance due to the magnetic properties of the steel core [34]. The current density J is dependent on the number of aluminium layers of the conductor [36].

$$R_{ac}(f, T_c, J) = R_{dc}(f_{60\text{Hz}}, T_{ref}) [1 + \alpha(T_c + T_{ref})(b + m \times J)] \quad (2.7)$$

f = Frequency at 60 Hz

J = Current density

b = constant, normally = 1

m = 0.018 for a three layer conductor

Most of the models that utilize the CIGRÉ method omit the magnetic flux density factor from the AC resistance calculations and use the skin effect factor [30]. The AC resistance equation used in such models is shown in equation (2.8).

$$R_{ac}(f, T_c, J) = R_{dc}(f_{60\text{Hz}}, T_{ref}) [1 + \alpha(T_c + T_{ref})] k_f \quad (2.8)$$

The IEEE method uses two measured values of resistances obtained from the conductor manufacturers [29]. The AC resistances are measured at 25 °C and 75 °C depicted as $R(T_{Low})$ and $R(T_{High})$ respectively in equation (2.9). The AC resistance at any conductor temperature T_c is then calculated by linear interpolation using equation (2.9).

$$R_{ac}(T_c) = \frac{R(T_{High}) - R(T_{Low})}{T_{High} - T_{Low}} \cdot (T_c - T_{Low}) + R(T_{Low}) \quad (2.9)$$

T_{Low} = Low temperature at which the first conductor AC resistance is measured

T_{High} = High temperature at which the second value of the AC resistance is measured.

2.4.3. Solar Heat Gain

The IEEE method defines the rate of solar heat as equation (2.10) [29].

$$Q_s = \alpha_s Q_{se} \sin(\theta) A' \quad (2.10)$$

α_s = Solar absorptivity of conductor surface

A' = Projected area of conductor per unit length

Q_{se} = Total heat flux elevation correction factor. Tables are presented in [29] to define correction factor at different solar altitudes, azimuth and hour angles [29] [39].

θ = Effective angle incidence of sun's rays

$$\theta = \cos^{-1}[\cos(H_c) \cos(Z_c - Z_l)] \quad (2.11)$$

H_c = Altitude of sun, defined in equation (2.12)

$$H_c = \sin^{-1}[\cos(Lat) \cos \delta \cos \omega + \sin(Lat) \sin \delta] \quad (2.12)$$

Z_c = Azimuth of sun, defined as equation (2.13)

$$Z_c = C + \tan^{-1}(\chi) \quad (2.13)$$

C = Solar azimuth constant

χ = Solar azimuth variable

$$\chi = \frac{\sin(\omega)}{\sin(Lat)\cos(\omega) - \cos(Lat)\tan(\delta)} \quad (2.14)$$

The relationship between the χ , C and ω is clearly presented in Table 2-1 [29].

Table 2-1: Solar azimuth constant, C , as a function of hour angle, ω , and solar azimuth variable

Hour Angle, ω (degrees)	C if $\chi \geq 0$ (degrees)	C if $\chi < 0$ (degrees)
$-180 \leq \omega < 0$	0	180
$0 \leq \omega \leq 180$	180	360

Z_l = Azimuth of the line

The CIGRÉ method defines the solar heat gain by equation (2.15). The angle at which solar heat is radiated to the conductor is not included in this equation. Both diffuse and direct radiations are considered [39].

$$Q_s = \alpha_s SD \quad (2.15)$$

S = Global solar radiation

2.4.4. Convection Heat Loss

Convective heat loss is as a result of air flowing over the outer surface of the conductor, causing cooling to the conductor by transferring the heat from the conductor surface to the surrounding air [40]. It is convection as natural convection and forced convection in both methods. Natural convection occurs when heat migrates from a hotter region to a cooler region until the temperature is uniform across the entire system without wind. [29] Forced convection is a result of wind. During forced convective cooling, the wind transfers heat from the conductor to the low temperature gradient of the air around the conductor [29].

The expressions for convective cooling for the IEEE method take the form of equations (2.16) and (2.17). Equation (2.16) describes the cooling effect due to natural response, with the wind speed quite low, below 0.5 m/s, and equation (2.17) is used for high wind speeds.

$$Q_{C1} = 1.01 + 0.0372 \left(\frac{D\rho_r V_w}{\lambda_f} \right) k_f k_{angle} (T_c - T_a) \quad (2.16)$$

$$Q_{C2} = 1.0119 \left(\frac{D\rho_r V_w}{\lambda_f} \right)^{0.6} k_f k_{angle} (T_c - T_a) \quad (2.17)$$

Q_{C1} = Convective cooling at low wind speeds

Q_{C2} = Convective cooling at high wind speeds

k_f = Thermal conductivity of air

k_{angle} = Wind direction

V_w = Wind velocity

ρ_r = Air density

D = Conductor outer diameter

λ_f = Dynamic viscosity

The dynamic viscosity and air density are functions of conductor temperature and ambient temperature. A value of 1 is used for perpendicular wind angle and 0.388 for parallel wind angle [41]. Hence, both the wind and transmission line directions are considered during the thermal rating calculations.

The wind angle, dynamic viscosity, thermal conductivity of air and air density are represented by equations (2.18), (2.19), (2.20) and (2.21), correspondingly [29] [30].

$$k_{angle} = 1.194 - \cos \theta + 0.194 \cos 2\theta + 0.368 \sin \theta \quad (2.18)$$

$$\lambda_f = \frac{1.458 \times 10^{-6} (T_f - 273)^{1.5}}{T_f + 383.4} \quad (2.19)$$

$$k_f = 2.42 \times 10^{-2} + 7.477 \times 10^{-5} T_f - 4.407 \times 10^{-9} T_f^2 \quad (2.20)$$

$$\rho_r = \frac{1.293 - 1.525 \times 10^{-4} H_e + 6.379 \times 10^{-9} H_e^2}{1 + 0.00367 T_f} \quad (2.21)$$

H_c = Elevation of conductor above sea level and is given by equation (2.22).

$$H_c = \sin^{-1} [\cos(Lat) \cos \delta \cos \omega + \sin(Lat) \sin \delta] \quad (2.22)$$

Lat = Degrees of latitude

ω = Hour angle which is set at 15° at noon and 30° at 2 p.m.

δ = Angle given by equation (2.23)

$$\delta = 23.4583 \sin\left[\frac{284 + N}{365} 360\right] \quad (2.23)$$

N = Day of the year

The CIGRÉ method computes convective cooling using equation (2.24). Forced and natural convection are differentiated through the Nusselt number N_μ .

$$Q_c = \lambda_f \pi (T_c + T_a) N_\mu \quad (2.24)$$

The Nusselt number is a dimensionless parameter which is determined from the Reynolds, Grashof and Prandtl numbers. The Reynolds number is a function of wind speed, air density and the kinetic viscosity of air. The Grashof number is a function of kinetic viscosity, conductor diameter, ambient and conductor average temperatures. The Prandtl number is calculated from experimental equations [30] [26].

The Nusselt number for natural convection is presented in equation (2.25).

$$N_\mu = A_2 (G_r P_r)^{m_1} \quad (2.25)$$

The Grashof and Prindtl numbers that correspond to the Nusselt number for natural convection energy calculation are defined by equations (2.26) and (2.27).

$$G_r = \frac{D^3 g (T_c - T_a)}{(T_f + 273) \nu_f^2} \quad (2.26)$$

$$P_r = \frac{c \mu_f}{\lambda_f} \quad (2.27)$$

The Nusselt number for the CIGRÉ's forced convection expression is given by equation (2.28) and the corresponding Reynolds number is presented by equation (2.29).

$$N_\mu = B_1 R_e^n \quad (2.28)$$

B_1 and n are constants that are dependent on the Reynolds number and the roughness factor of the conductor. The CIGRÉ model provides a table with the constants at given Reynolds numbers and conductor roughness factors [30].

$$R_e = \frac{\rho V R_e^n}{\nu_f} \quad (2.29)$$

V = Wind velocity

The relative air density, ρ_r , used in the calculation of the Reynolds number is given by equation (2.30).

$$\rho_r = \frac{\rho}{\rho_o} \quad (2.30)$$

ρ = Air density at a given altitude

ρ_o = Air density at sea level

2.4.5. Radiative Heat Loss

Both models use the same expression for radiative cooling, presented in equation (2.31), as a function of conductor diameter, emissivity, conductor temperature and ambient temperature.

$$Q_r = 0.0178D\varepsilon \left[\left(\frac{T_c - 273}{100} \right)^4 - \left(\frac{T_a - 273}{100} \right)^4 \right] \quad (2.31)$$

ε = Emissivity of conductor surface

Emissivity depends on the conductor surface roughness, and increases with age [8] [42]. It varies from 0.27 for new conductor to 0.95 for field exposed worn conductors [42]. If the emissivity of a conductor is unknown, a value of 0.5 is suggested [29] [30].

2.4.6. Thermal Ratings Calculations

The thermal rating or ampacity of overhead conductors is hereafter calculated by solving for the current, I in equation (2.1) in terms of weather-related information. An iteration process is employed in the calculation of the current because the relationship between the conductor temperature, radiation and convective heat losses is not linear [43].

2.5 Meteorological Information for steady state thermal rating

As shown from the equations for calculating the current-temperature relationship in section 2.4, the conductor temperature depends on the weather conditions of the environment where the transmission line is built. Weather conditions essentially affect the thermal behaviour of the conductor and should be chosen carefully for conductor thermal rating calculations [27] [44]. The weather data that principally affect thermal rating are ambient temperature, wind speed and direction, and global solar radiation [27] [45].

Three methods are generally used for weather data predictions [10]. These methods include the deterministic method, probabilistic method and dynamic method. The deterministic method assumes extreme weather information based on the weather patterns in the area where the transmission line will be built, and effectively, some engineering judgment [45]. The probabilistic method uses forecasted weather information obtained from weather stations to determine the probability of occurrence [10] [44] [46]. The most likely weather case is used for the thermal rating calculations. The dynamic method works with real time monitoring systems and sensors installed on the transmission line to regularly record the weather data and link it to the transmission line control stations [10] [47]. The current loading on the line is therefore adjusted periodically as the weather data changes.

The CIGRÉ TB299 document suggests that extreme weather conditions or the deterministic method be taken into consideration for the calculation of thermal ratings of new conductors to be used for general purposes. The extreme weather information is normally suggested based on engineering judgment obtained from weather stations [44]. It must be noted that the deterministic computation of conductor thermal ratings result in underutilization of the conductors [48], hence for specific line rating probabilistic and dynamic rating methods should be used [48].

Careful selection of weather parameters for thermal rating calculations is as important as the selection of method of calculation itself and requires considerable engineering judgment [49] [10]. The weather data include the ice thickness, ice density, and the wind speed at a given ambient temperature which define the designed maximum weather loading [48] [49]. Wind speed is the most varying parameter and the most important determinant of ratings [10] [49].

Thermal ratings of conductors determine the absolute maximum working tension that the conductors may experience and, therefore, the maximum sag value developed at certain conductor temperatures.

2.6 Previous Electrical Studies on RW and TW Conductors

Electrical performance comparisons have been done extensively mostly on ACSR versus AAC and HTLS conductors and documented in [7] [8] [50] [51] [52] [53]. Most of the performance comparisons between conductor forms of RW and TW are on vibration and corrosion tests. There are a few comparisons on the current carrying capacities of ACSS and ACSR in TW and RW conductors discovered during the literature survey.

In [19], self-damping, power dissipation, sag-tension and current carrying capacities of ACSR and ACSS conductors in RW and TW forms comparisons were performed. A test line was used

where the aim was to increase the current carrying capacity of the line. Two options were investigated. The first option was to tension the existing ACSR/RW conductor at 50 % of its rated ultimate tension (RTS). The second option was to use ACSS/TW conductor. The results from both options were compared: with the use of ACSR/RW, the current carrying capacity at the same sag increased to 39 % at a conductor temperature of 100 °C. However, the structures needed to be modified to accommodate 30 % increase in transverse loads. With the use of ACSS/TW conductor, the current carrying capacity increased by 70 %, at conductor temperature of 180 °C. The increase was achieved without structural modifications. It was concluded that with the use of ACSS/TW conductors a cost saving of 20 % is achieved when compared to ACSR/RW conductors.

A performance comparison on ACSS and ACSR conductors was conducted in [20]. The comparisons were done through installing the conductors in five different fields and through laboratory evaluations. The ACSS conductor was found to perform better than ACSR conductor with respect to resistance to aeolian vibrations, sag at high temperatures, high temperature capability and longtime creep.

It was found in [17] that ACSS in TW form offered significant increase in power transfer capabilities than a RW version of ACSS. EPRI [54] reported that TW conductors have less resistance and more current capacity than the ACSR RW conductor counterpart, which allows improved efficiency and utilization of the right of way. However, there were no results recorded in [54] to ascertain the report. Moreover, the South African weather assumptions were not taken into consideration when the studies were done.

In [8], it was emphasized that there is limited published work conducted on performance comparisons on actual transmission line structures. Through the literature survey conducted, the comparisons of RW and TW forms in terms of magnetic fields and power losses were not found. The work that relates thermal ratings and sag performances on a real line is done on AAAC and ACSR conductors and is limited to 33 kV wood poles [8]. Therefore, this work defines the critical properties of TW and RW conductors and how they affect the electrical performance of the conductor in terms of ampacity, power losses, and magnetic fields.

2.7 CONCLUSION

There have been numerous studies done on overhead conductors to determine the thermal ratings of ACSR versus ACSS conductors. Most of the conclusions made in such studies do not quantify the benefits of using TW over RW in terms of power transfer capabilities measured by the current carrying capacities and the power losses of these conductors.

Previous studies on the subject of RW versus TW revealed gaps in the quantification of thermal ratings and power loss differences between the two conductor shapes. The studies also showed that the real limiting factor and the basis for line rating is the ability of the designed line to maintain safe clearance between energized conductors and the ground objects directly below the line. This has a direct impact on public safety. Furthermore, the magnetic fields as a result of sagged conductor need to be quantified to ensure public safety.

ACSS conductors have been shown to possess physical properties that are very similar to ACSR conductors but have the potential of offering better thermal ratings when compared to the conventional ACSR conductors.

It was noted that the replacement conductor used in reconductoring an existing transmission line should be capable of carrying more electrical current with the same or less maximum sag as the original conductor. To accomplish this, the replacement conductor should have characteristics such as low thermal elongation, low initial sag and low plastic elongation. RW and TW conductors have different thermal and plastic elongation characteristics which suggest that there could be differences in the current carrying capacities between the shapes.

The CIGRÉ and the IEEE methods have been identified as most used models for evaluating thermal ratings of conductors. Simulation programs in favor of both methods have been developed to be used to enable comparisons of the CIGRÉ and the IEEE methods.

Chapter 3

METHODOLOGY

3.1 Background

The main purpose of the study is to firstly evaluate the thermal ratings of the conductors to determine and compare the amount of current that the TW and RW conductors, in ACSR and ACSS types, are supposed to carry at the maximum temperature. Thereafter, the magnetic fields and the power losses are evaluated using the calculated maximum conductor current and the conductor resistance at respective temperatures. In this chapter, the methods and materials used for the study are described.

The estimation of thermal ratings, power losses and magnetic field comparisons were computed using two different types of ACSR and ACSS conductors namely: Tern (45Al. /7St.), and Martin (59 Al. /19 St.) [40]. Martin conductor was used because of its similar electrical properties to Bersfort (54 Al. /7 St.) [40]. In South Africa, Tern and Bersfort conductors are the most commonly used transmission line conductors in high voltage and extra high voltages (EHV) between 400 kV and 765 kV and are used in different bundle configurations.

The conductors' characteristics and cross section configurations are shown in Figure 3-1 and Table 3-1. Martin and Tern in ACSR and ACSS, RW and TW form conductor are composed of three layers of aluminium wire with (1350 H19 for ACSR and 1350 OH for ACSS) a high-strength galvanized steel core. The core of Tern conductor contains 7 steel wires and Martin has 19 steel wires [40].

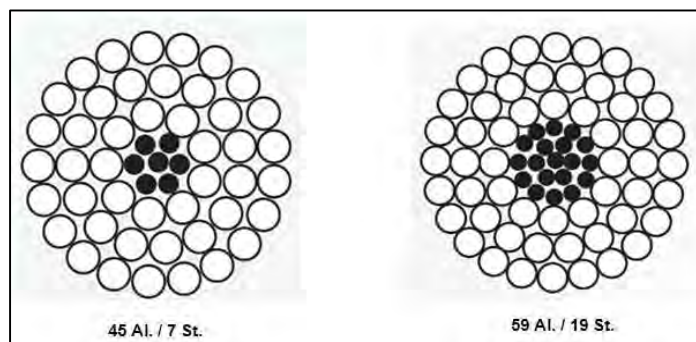


Figure 3-1: Tern and Martin RW conductor stranding [40]

45Al. /7St. = 45 aluminium strands and 7 steel strands.

59 Al. /19 St. = 59 aluminium strands and 19 steel strands.

3.2 RateKit

The thermal rating calculations were computed using RateKit version 5.0, developed by Nexans Cables Company. RateKit performs both steady state and transient thermal ratings. In steady state rating, either the conductor temperature for a specific conductor current is evaluated or the ampacity for a particular conductor temperature is calculated. In this study, the steady state conductor ampacities were calculated for conductor temperatures ranging from 50 °C to MCT conductor temperatures using both IEEE and CIGRÉ models presented in section 2. The MCT for the conductors used are listed in Table 3-1.

When used for steady state ampacity calculations, RateKit requires inputs such as the weather environment of the transmission line on which the conductors will be strung, conductor data, conductor temperature and a selection of the thermal rating model to be used. The outputs from the program are the steady state thermal rating or ampacity in amps, and the components of the heat balance equation, Q_s , Q_c and Q_r . Figure 3-2 shows the overview assimilation of the weather assumptions and the conductor data inputs with the methods for conductor thermal rating calculations in RateKit.

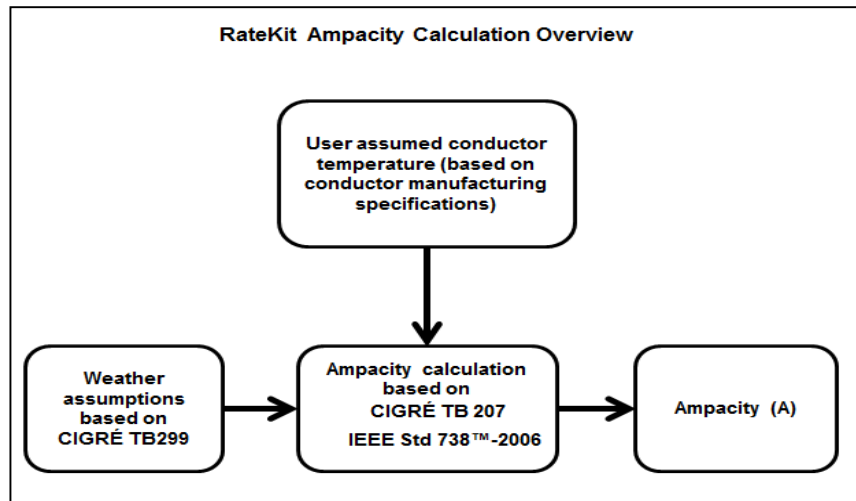


Figure 3-2: Thermal rating calculation overview in RateKit [5] [29] [45]

RateKit has a built-in conductor file that has the conductor data needed for thermal ratings calculations. The data include conductor diameters, aluminium and steel areas, strand ratio and the resistance at 25 °C and 75 °C. The file makes provision for the user to input the m and b values to enable resistance calculations taking into consideration the magnetic properties of the steel core according to the CIGRÉ method. The resistance is calculated according to equation (2.7).

Table 3-1: Tern and Martin Conductor Parameters [20] [40] [55]

Conductor Name	Tern				Martin			
Type	ACSR		ACSS		ACSR		ACSS	
Shape	RW	TW	RW	TW	RW	TW	RW	TW
Conductor Diameter (mm)	27.0002	24.3078	27.0002	24.384	36.1696	33.02	36.1696	33.02
Al Area (mm ²)	403	403	403	403	685	685	684.8	684.84
Total Area (mm ²)	430.58	430.644	430.58	430.644	777.611	771.547	771.482	771.547
Al Coefficient of Thermal expansion	0.002304	0.002304	0.002304	0.002304	0.002304	0.002304	0.002304	0.002304
St Coefficient of Thermal expansion	0.001152	0.001152	0.001152	0.001152	0.001152	0.001152	0.001152	0.001152
UTS (N)	98305.7	96971.2	63164.7	63164.7	205953	208177	161026	161026

Chapter 3: Methodology

Conductor Name	Tern				Martin			
Type	ACSR		ACSS		ACSR		ACSS	
Shape	RW	TW	RW	TW	RW	TW	RW	TW
Maximum Conductor Temperature (MCT) (°C)	100	100	250	250	100	100	250	250
Unit weight (N/m)	13.0732	13.0542	13.0615	13.0032	25.3496	25.2752	25.319	25.2752
Al Final Modulus of elasticity (MPa/100)	517.106	517.106	521.415	521.415	490.906	49.906	484.011	484.011
St Final Modulus of elasticity (MPa/100)	124.795	124.795	123.244	123.244	215.806	215.806	212.358	212.385
Stranding Al/St Ratio	45/7	17/7	45/7	17/7	54/19	39/19	54/19	39/19
Number of Aluminium layers	3	2	3	2	3	3	3	2
AC Resistance at (25°C, 60 Hz) (Ω/km)	0.0736325	0.0721	0.071644	0.0712713	0.0441174	0.0440052	0.0429989	0.0427503

Conductor Name	Tern				Martin			
Type	ACSR		ACSS		ACSR		ACSS	
Shape	RW	TW	RW	TW	RW	TW	RW	TW
AC Resistance at (*MCT, 60 Hz) (Ω /km)	0.088359	0.0863	0.137267	0.134838	0.0535622	0.0534269	0.0522573	0.0520088

* MCT is the maximum conductor operating temperature

3.3 Method for calculating Magnetic fields

Power line magnetic fields are calculated using the Biot-Savart's law either by numerical methods or by summation of the magnetic field contributions of each phase through superposition hypothesis [56] [57]. Numerical methods do not explicitly relate the magnetic field to the geometric characteristics of the line [56]. The approach taken for the calculation of magnetic fields in this study is based on the EPRI superposition method that assumes that: power frequency magnetic fields are only produced by the current on the conductor [58] [59]. The EPRI method is the one of the most widely used methods for calculating magnetic fields [60]. It is assumed that conductors form infinitely long straight parallel lines with each other and the ground plane [57] [61]. The depth of the image current is assumed to be too far below ground and hence it is neglected [57] [61]. Therefore the magnetic fields are calculated using Amperes law, given as equation (3.1) [13] [58] [59] [61].

$$B = \mu H \quad (3.1)$$

For a conductor at position (x_k, y_k) carrying a current of I_k , the horizontal and vertical components of the magnetic field B_x and B_y at a point are given as equation (3.2) [13] [61].

$$B_y = \frac{\mu I_k}{2\pi} \cdot \frac{(x_p - x_k)}{R^2} \quad (3.2)$$

$$R^2 = (x_p - x_k)^2 + (y_k - y_p)^2 \quad (3.3)$$

$$B_{xp} = B_{rxp} + jB_{ixp} = \sum_k \frac{\mu(I_{rk} + jI_{ik})}{2\pi} \cdot \frac{(y_k + y_p)}{R^2} \quad (3.4)$$

$$B_{yp} = B_{ryp} + jB_{iyp} = \sum_k \frac{\mu(I_{rk} + jI_{ik})}{2\pi} \cdot \frac{(x_p + x_k)}{R^2} \quad (3.5)$$

μ = Permeability of material

R = Distance from magnetic field source (x_k, y_k) to the position of field measurement (x_p, y_p) .

The resultant value of the magnetic field is mostly used in engineering calculations and is given by equation (3.6).

$$B_{res} = B_{ryp}^2 + jB_{iyp}^2 + B_{rxp}^2 + B_{ixp}^2 \quad (3.6)$$

From equations (3.1) to (3.6), it is clear that there are two components that greatly affect the power frequency magnetic fields: the amount of current through the conductor and the position of the conductor. The magnitudes of the magnetic fields from the conductors are then defined based on the position of the conductor above ground, where there is potential hazard to public safety. For this reason, the magnetic fields in this study are investigated on a real Eskom transmission line, with all its parameters so that the positions of the TW and RW conductors are well defined by the conductor attachment heights, provided by the tower structures used to support the conductors.

3.3.1. Transmission Line Parameters

Particular reference was made to an Eskom 400 kV power line called Apollo - Verwoerdburg for the magnetic fields evaluations. The line was simulated using PLS-CADD program and the magnetic fields were thereafter evaluated.

The detailed design for the 400 kV line from Apollo to Verwoerdburg substation is documented in [62]. Apollo-Verwoerdburg is a very short link between Apollo and Verwoerdburg substations of about 2.5 km that was designed from a cut-off of an existing Eskom line called Apollo-Pluto 400 kV line. At the time that the line data was obtained, Apollo-Verwoerdburg was still in the design stage, to be constructed by mid-2014. The line was designed with 518H, 518C and 518D structures, strung with $4 \times$ Bear conductors with two fiber optic ground wires (OPGW), for the 2.5 km length of the line. The structures were insulated with glass cap and pin insulators. The line was designed with a ground clearance of 10 m to minimize fire related faults. The electrical loading of the line was forecasted at 714 MW and 980 MW for normal and contingency conditions respectively.

The design parameters of the line are presented in Table 3-2. The tower outline drawings used for the purposes of this study are presented in Appendix B. Figure 3-3 shows the Google Earth map for the location of the line route.

Table 3-2: Apollo-Verwoerdburg 400 kV line design parameters

Towers	Conductors	Ground-Wires	Line Electrical Loading (MW)	Insulators
426A, 518C, 518D, 520B	$4 \times$ Bear	$2 \times$ 24 core OPGW	714	Glass



Figure 3-3: Google Earth map showing the line route for Apollo-Verwoerdburg 400 kV Line

3.3.1. Structures for Apollo - Verwoerdburg Line

The 5xx series of structures are used in Eskom to designate 400 kV transmission line structures [40]. The letters A, B, C, D, etc. indicate that the structures are either suspension or angle (strain) structures. Suspension structures are normally denoted by the letters A and B. Letters C, D, E and F denote strain structures [40]. Suspension and dead-end structure examples are shown in Figure 3-4. The main differences between the letters denoting the structures are the structures geometry such as attachment height limits, phase spacing, line angles, design loads, and tower top geometries. Such information is captured in the tower outline drawings presented in Appendix B and summarized in Table 3-3.

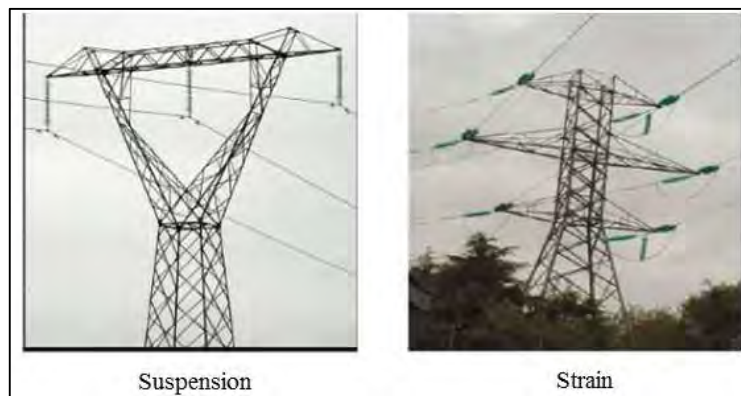


Figure 3-4: Example of Suspension and dead-end structures [63]

Apollo – Verwoerdburg line uses the 520B guyed-v suspension structures and the 518C and 518D strain self-supporting structures. The 518D structure is also used as a terminal structure. A

terminal structure is the last structure that terminates the transmission line before the gantry at the substation. All the structures are of horizontal or flat configuration. Appendix B shows the outline drawings of the structures used for the line. The outline drawings indicate the dimensions of conductor attachment heights, phase-to-phase and phase-to-earth clearances in millimeters.

Table 3-3, outlines the maximum wind and weight spans of the structures used for the study. The angles presented in the Table are the angles that the structures can be spotted at without exerting excessive strain. For instance, the 518C structure can withstand loads if used for angles between 0° and 35°. The wind and weight span values were obtained from LES and calculated using a Tower Loader program developed by Eskom engineers. The calculations are based on the IEC standard [64] and SANS 10280 [65].

Table 3-3: Structure information used in PLS-CADD

Tower Type Name	Description	Max. Wind Span (m)	Max. Weight Span (m)	Max. Uplift Span (m)
520 B	SUSPENSION, SELFSUPPORTING	500	900	-
518 C	0°-35° ANGLE STRAIN	500	1200	200
518 D	(a) 35°- 60° ANGLE STRAIN	500	1200	200
	(b) 0° TERMINAL	375	1200	200

3.3.2. Conductor Data used in PLS-CADD

The conductor specifications presented in Table 3-1 and the PLS-CADD conductor files of both Tern and Martin conductor of ACSR and ACSS types, in RW and TW forms were provided by Southwire conductor manufacturing company.

The required information for the evaluation of magnetic fields in PLS-CADD include the conductor files presented in Appendix A and the conductors parameters described in section 3.2. The essential conductor parameters required for magnetic field simulations are the mean conductor diameter, resistance, the number of sub-conductors in the conductor bundle. The

current in each phase of the conductor is also needed as input to the program. In PLS-CADD, the mean diameter for a bundled conductor is calculated using on equation (3.7), according to the EPRI method.

$$d_s = s \times \sqrt{2} \quad (3.7)$$

d_s = Mean conductor diameter

$$s = \text{sub-conductor spacing} = 17 \times D \quad (3.8)$$

3.4 Conclusion

This chapter presented the methods and the software programs used for the electrical characteristic comparisons between TW and RW conductors. The RateKit versions 5 software to calculate and compare the thermal ratings of the conductors was described. The EPRI method used to evaluate the magnetic fields was defined. The properties of a 400 kV transmission line used as a case study where the conductors are strung and the magnetic fields emitted from the line are analyzed and the materials used for the study were highlighted. The data used, i.e. conductor files and structure files, for the PLS-CADD program was specified. The conductor properties of TW and RW; and ACSS and ACSR conductors were defined.

Chapter 4

ELECTRICAL ANALYSIS OF TW AND RW

4.1 INTRODUCTION

In this chapter, the thermal ratings, power losses and magnetic fields of ACSS and ACSR in TW and RW shapes are quantified. The ampacity and power losses from the conductors are plotted as functions of conductor temperature. The magnetic fields are related to the current carrying capacities of the conductors. Tern and Martin conductors in both ACSR and ACSS conductor types are used in all the electrical studies performed. Section 4.2 presents the differences between the CIGRÉ and the IEEE methods in the calculation of thermal ratings - it is essential that the methods be compared first to determine which method will work best for the study. In section 4.3, the thermal ratings of TW versus RW; and ACSR versus ACSS conductors; using the CIGRÉ method are presented. The magnetic fields comparisons between RW and TW are evaluated after calculating the thermal ratings of the conductors, and the results are presented in section 4.6.

4.2 CIGRÉ versus IEEE in Ampacity Calculations

It was realized in section 2.2 that the major differences between the IEEE and CIGRÉ methods are more pronounced in the convective cooling and solar heating equations, and the calculations of the AC resistances. Graphs showing the relationship between ampacity versus conductor temperature for both the methods are presented. The comparison between IEEE and CIGRÉ models is made through amounts of heat dissipated and absorbed by the conductors. The ACSR and ACSS, Tern and Martin conductors are used as reference under the conditions shown in Table 4-1 based on the worst weather cases as advised by SANS 10280 and the CIGRÉ 299 document [45] [66]. Table 3-1 presents the physical properties of the conductors used for the study in TW and RW counterparts.

Table 4-1: Meteorological input assumptions [45] [66]

α_s	ϵ	Air Temp. (°C)	Wind Speed (m)	Wind Angle (deg)	Elevation above sea (m)	Latitude (deg)	Conductor Orientation (deg)
0.5	0.5	40	0.6	90	1500	30	90

Figure 4-1 to Figure 4-4 illustrate the behaviour of the conductors' ampacity in relation to the conductor temperature variations for the CIGRÉ and IEEE methods with Tern ACSR and ACSS conductors in TW and RW shapes. The IEEE method allows for simulations to be done in clear and industrial conditions [29]. Clear conditions imply rural environment where there are no industrial pollution affecting the conductor's roughness factor. Industrial conditions denote places where there are industrial activities affecting the atmosphere and hence the conductor roughness factor.

The results in Figure 4-1 show 56 % discrepancies in the ampacity comparisons between the models with the use of Tern ACSR conductor in RW shape at conductor temperatures below 60 °C. In all instances, i.e. Figure 4-1 to Figure 4-4, the results are consistent in that, at conductor temperatures below 60 °C, the IEEE industrial method resulted in more conservative results. However, at conductor temperatures above 60 °C, the CIGRÉ method gave the most conservative results. The results obtained with Tern ACSS conductor in both RW and TW shapes showed significant differences of 2.5 % at temperatures above 190 °C. The IEEE in both industrial and clear conditions produced very close to similar results in temperatures above 190 °C for Tern ACSS conductor in both RW and TW forms.

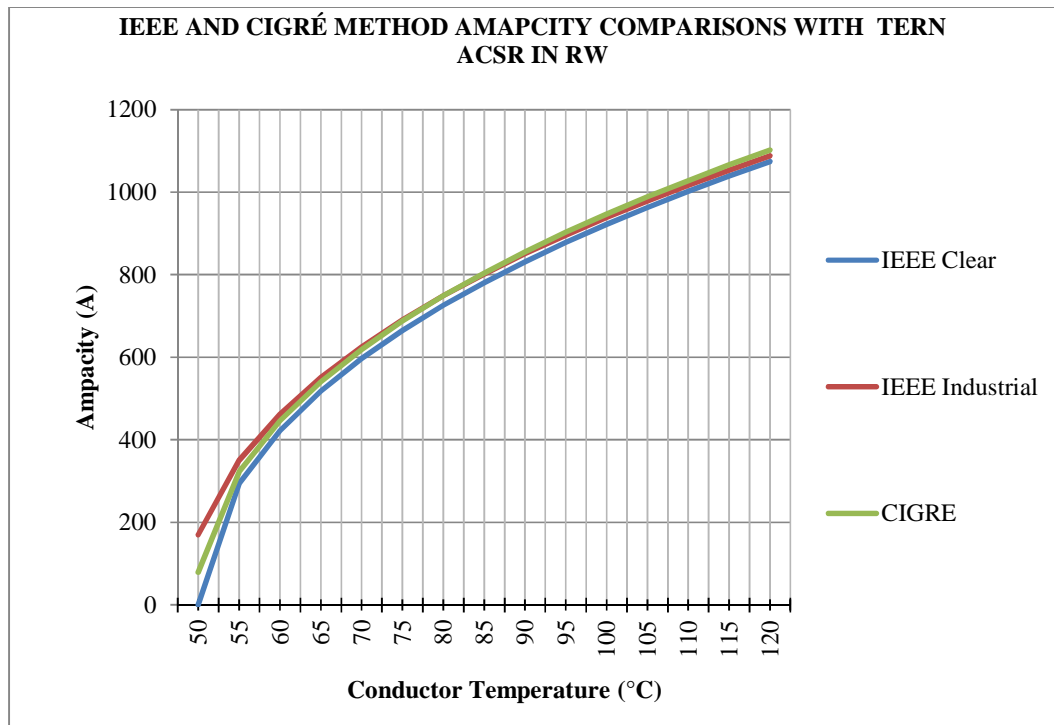


Figure 4-1: IEEE and CIGRÉ models comparison with Tern ACSR conductor in RW shape

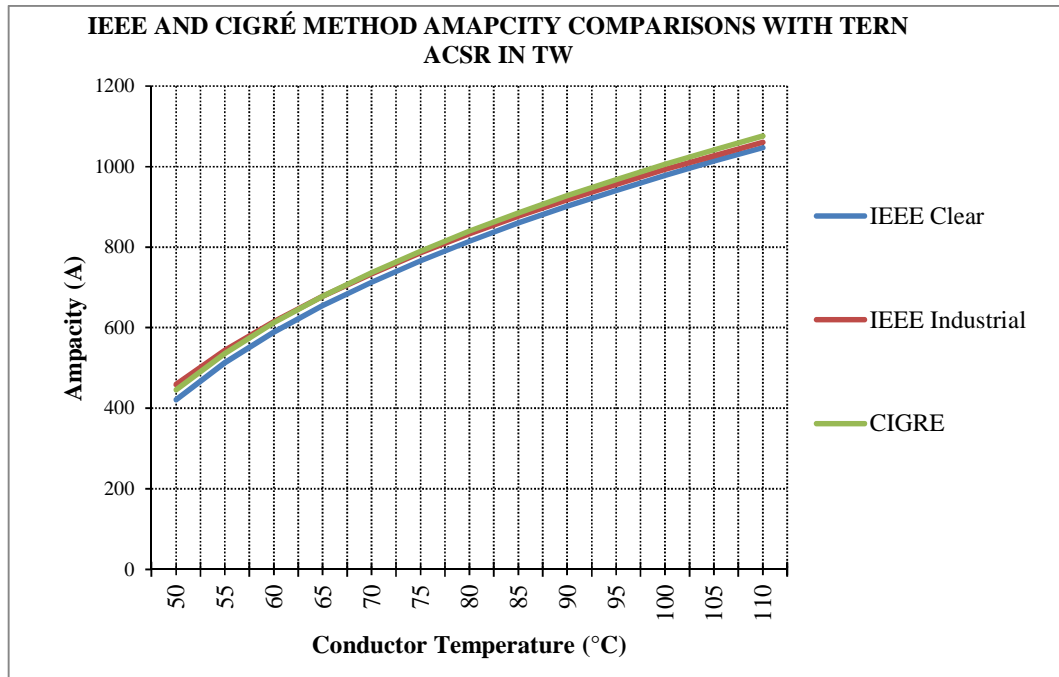


Figure 4-2: IEEE and CIGRÉ models Comparison with Tern ACSR conductor in TW shape

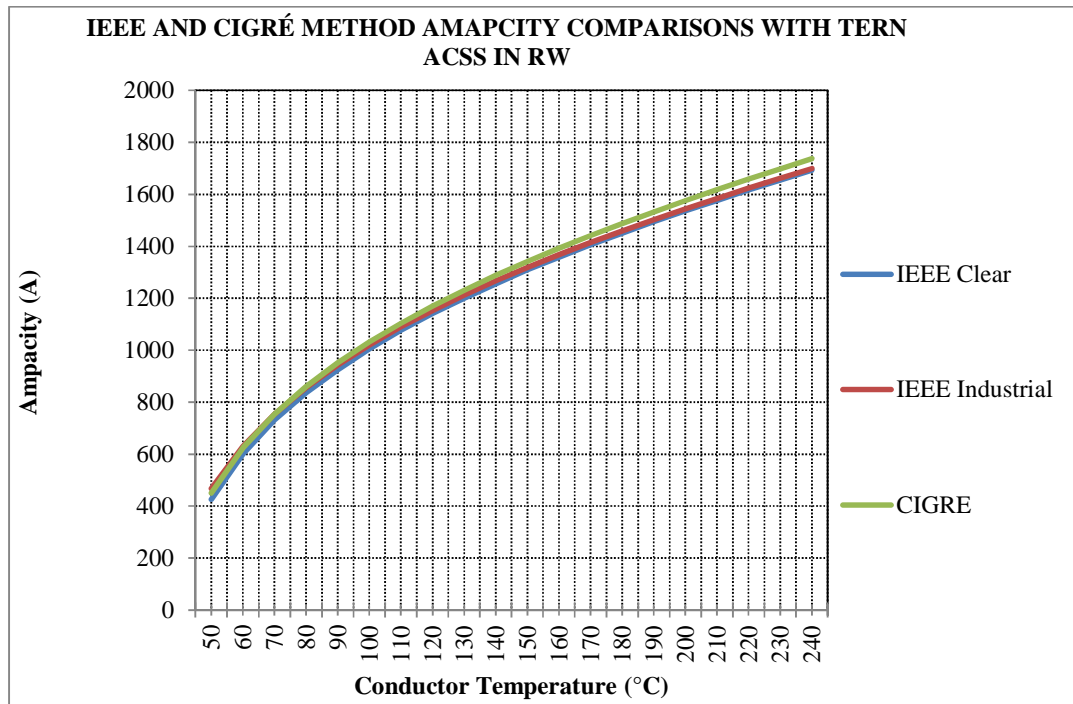


Figure 4-3: IEEE and CIGRÉ models comparison with Tern ACSS conductor in RW shape

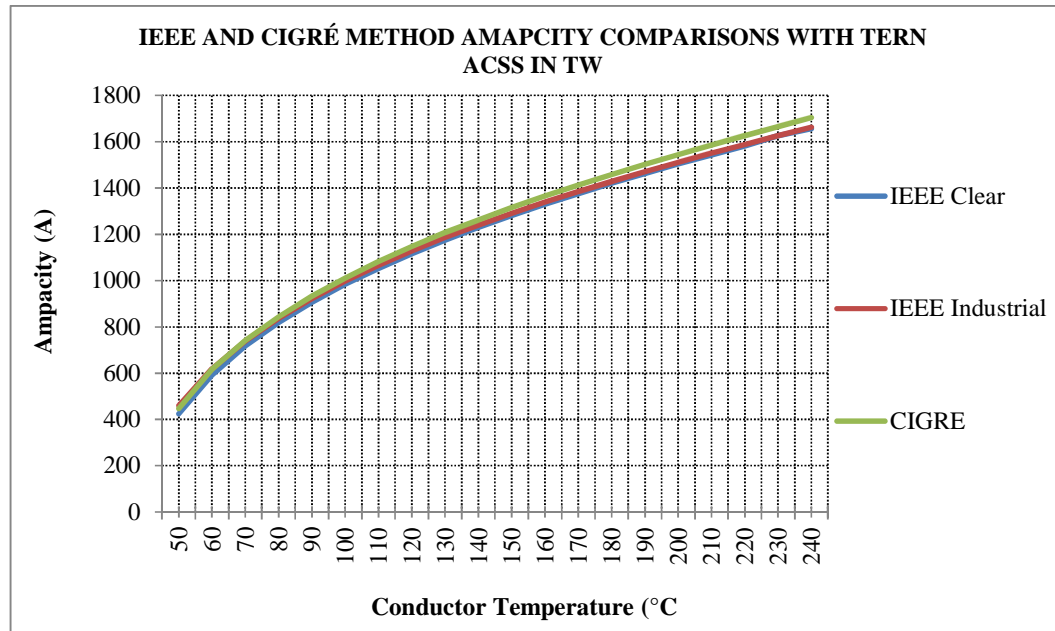


Figure 4-4: IEEE and CIGRÉ models comparison with Tern ACSS conductor in TW shape

The results computed with Martin conductor in ACSR and ACSS types under the same assumptions made in Table 4-1 are presented in the charts from Figure 4-5 to Figure 4-8. The difference between the ampacity calculated for the CIGRÉ and the IEEE models is approximately 50% for the conductors at temperatures below 70 °C. Both IEEE and CIGRÉ models could not populate any ampacity values when the conductor temperature was set to 50 °C and below, at the wind speed of 0.6 m/s. As shown in the plots different conductors under the same conditions showed dissimilar results at conductor temperatures below 60 °C. The difference between the obtained values for the CIGRÉ and IEEE models was approximately 16 % for the ACSR Martin conductor at conductor temperatures below 60 °C.

The percentage differences in ampacity of the models are shown in Figure 4-9. The ampacity differences observed when comparing CIGRÉ and IEEE industrial were about 8 % at conductor temperature of 50 °C. The ampacity differences between CIGRÉ and IEEE industrial models reduced to 0 % at conductor temperatures between 70 °C to 85 °C. The differences between IEEE in clear and IEEE in industrial conditions range from 4% to 16 % within conductor temperatures of 50 °C to 70 °C and decreases to almost 2 % at conductor temperatures of 80 °C to 100 °C. The differences between the CIGRÉ and IEEE in clear conditions methods stabilized to 3 % between the conductor temperatures of 70 °C to 100 °C.

Similar results patterns are observed with Tern ACSS conductor in Figure 4-10, where the differences between the CIGRÉ and IEEE industrial models stabilized to 2 % at conductor

temperatures of 60 °C to 250 °C. The ampacity differences between CIGRÉ and IEEE clear models became stable to 2.5 % at temperatures between 100 °C to 250 °C.

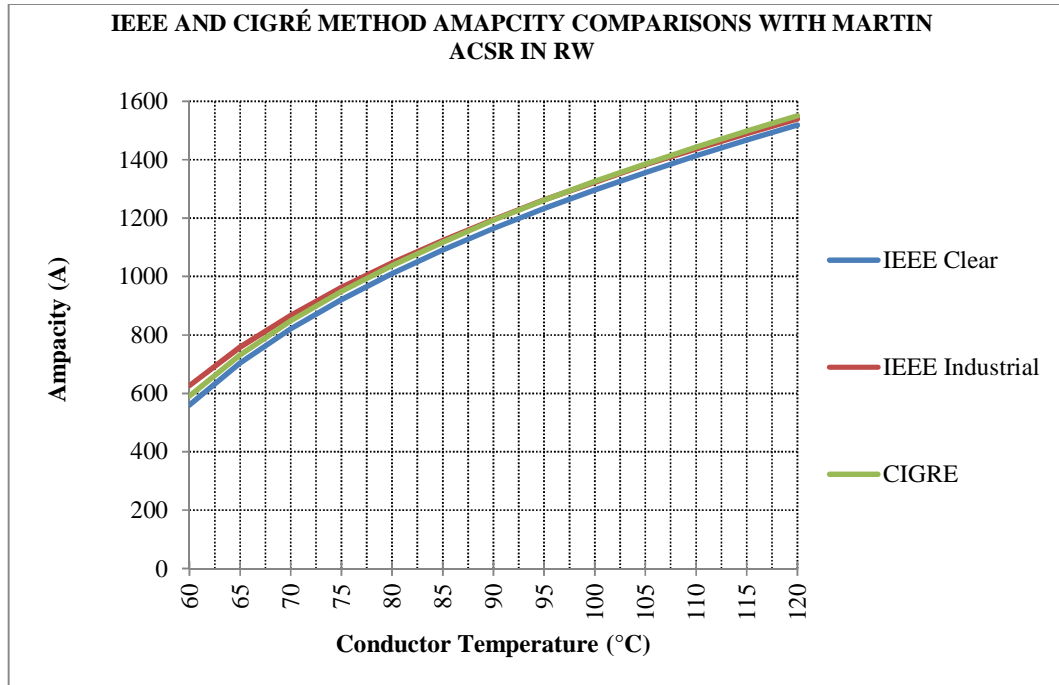


Figure 4-5: IEEE and CIGRÉ models comparison with Martin ACSR conductor in RW shape

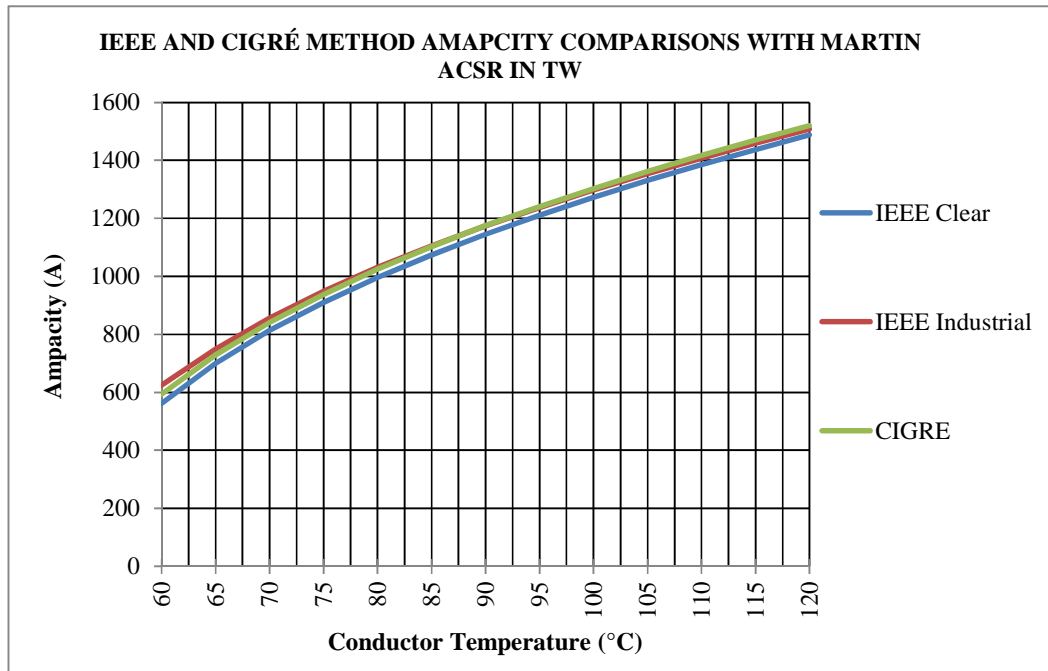


Figure 4-6: IEEE and CIGRÉ models comparison with Martin ACSR conductor in TW shape

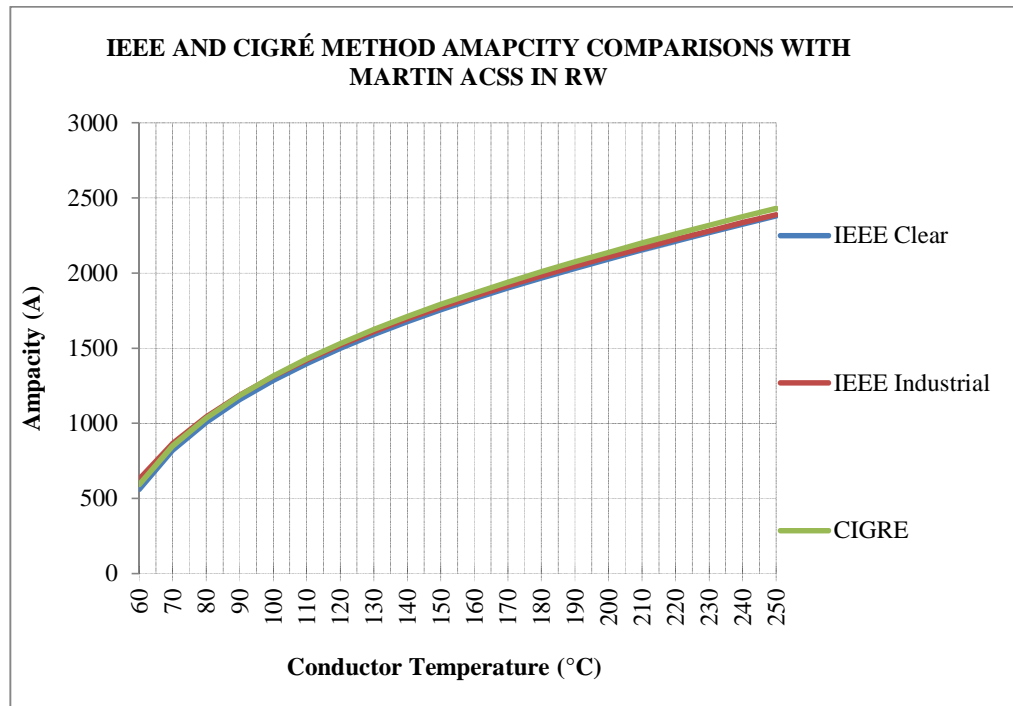


Figure 4-7: IEEE and CIGRÉ models comparison with Martin ACSS conductor in RW shape

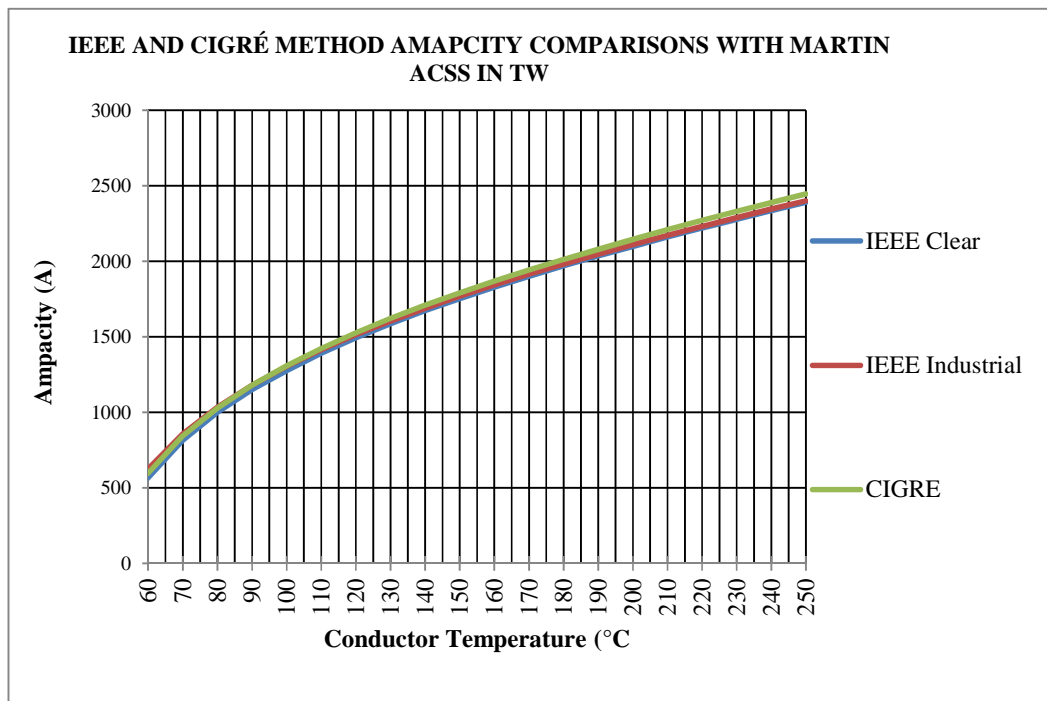


Figure 4-8: IEEE and CIGRÉ models comparison with Martin ACSS conductor in TW shape

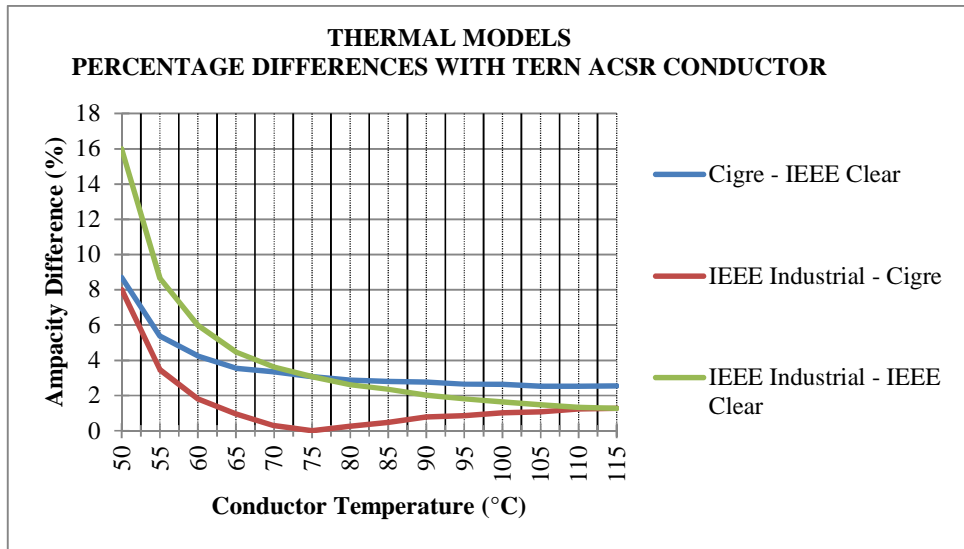


Figure 4-9: Ampacity difference percentages of thermal models with ACSR conductor

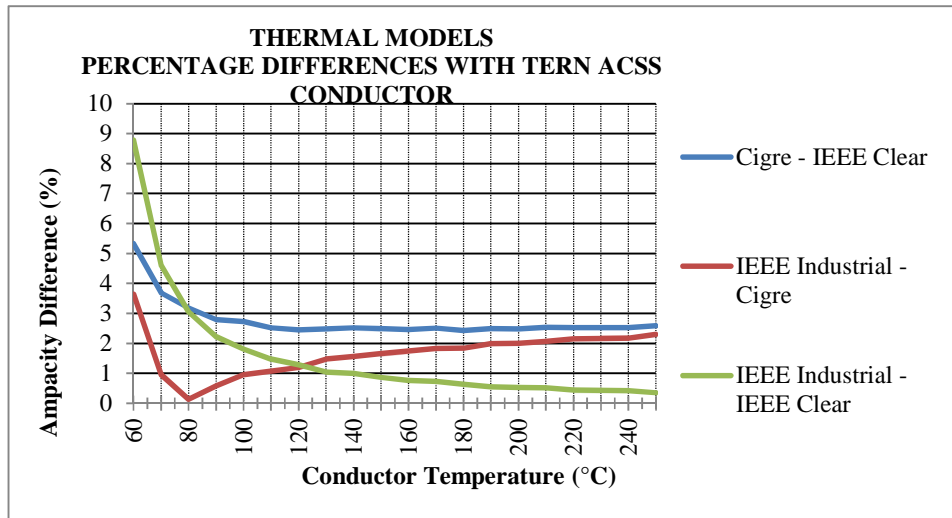


Figure 4-10: Ampacity difference percentages of thermal models with ACSS conductor

From the results in Figure 4-9 and Figure 4-10; it is observed that the differences between the models are very minimal. This proves that either the IEEE or the CIGRÉ models can be used for calculating the ampacities of conductors. Although the IEEE method was said to make provision for elevated temperature ampacity computations as stipulated in [26], this advantage over the CIGRÉ model is not visible from the presented results.

The ampacity differences between clear and industrial conditions of the IEEE method are more pronounced at temperatures below 100 °C and become almost zero as the temperatures reach 250 °C. This shows that at high temperatures, the line environment, industrial or clear, will not have a significant impact on the ampacity calculations.

The major contributors towards the differences between the ampacity models are solar heating, convective cooling and AC resistances. The differences in the heat equation components is shown clearly in the tables below, from Table 4-2 to Table 4-5 . The discrepancies between heat components increase with the conductor temperature and conductor diameter. The conductor temperatures were chosen randomly at 70 °C for ACSR conductor and 150 °C for ACSS conductors in RW forms. The difference in AC resistance is about 1.8 % at the conductor temperature of 70 °C between the two methods. Similar results patterns are observed in all tabulated results, that the largest contributor of the differences between the models is convective cooling.

Table 4-2: Heat energy components with Tern ACSR RW conductor at $T_c = 70$ °C

Model	Q _s (Watts/m)	Q _c (Watts/m)	Q _r (Watts/m)	AC Resistance (Ω)	Ampacity (A)
IEEE	15.88	36.37	10.21	0.08099	597
CIGRÉ	15.3	38.17	10.21	0.08253	619

Table 4-3: Heat energy components with Martin ACSR RW conductor at $T_c = 70$ °C

Model	Q _s (Watts/m)	Q _c (Watts/m)	Q _r (Watts/m)	AC Resistance (Ω)	Ampacity (A)
IEEE	21.27	42.2	13.68	0.052618	821
CIGRÉ	20.49	43.8	13.68	0.053076	848

Table 4-4: Heat energy components with Tern ACSS RW conductor at $T_c = 150$ °C

Model	Q _s (Watts/m)	Q _c (Watts/m)	Q _r (Watts/m)	AC Resistance (Ω)	Ampacity (A)
IEEE	15.88	133.07	53.93	0.108098	1256
CIGRÉ	15.3	141.22	53.93	0.109765	1288

Table 4-5: Heat energy components with Martin ACSS RW conductor at $T_c = 150\text{ }^\circ\text{C}$

Model	Q_s (Watts/m)	Q_c (Watts/m)	Q_r (Watts/m)	AC Resistance (Ω)	Ampacity (A)
IEEE	21.27	126.27	72.25	0.067856	1756
CIGRÉ	20.49	134.6	72.25	0.070169	1792

4.3 Effect of Temperature on Resistance

Figure 4-11 and Figure 4-12 show the AC resistance dependency on temperature for ACSR and ACSS conductors of different diameters, correspondingly, for the IEEE and the CIGRÉ models. The results show that the resistance is linearly dependent on the temperature for both methods. There is a close correlation between the two models for both Martin and Tern conductors in ACSR and ACSS types. Martin conductor has lower resistance compared to Tern conductor although the diameter of Martin is larger than that of Tern conductor.

The AC resistance differences between the IEEE and CIGRÉ methods for ACSR conductors range from 1.8 % to about 2.2 % when Tern conductor is used. With the use of Martin ACSR conductor, the difference in AC resistance ranges from 0.01 % to 1.2 %. At temperatures below $100\text{ }^\circ\text{C}$, the resistance differences between TW and RW of the same conductor type are almost similar but diverge as the temperatures increase. This is more pronounced with Martin ACSS conductor. The ACSS conductors showed differences as high as 4 % for Martin conductor and for Tern conductor the differences were within 2.7 %. The CIGRÉ method had the highest AC resistance values.

The work done by [67], on the subject of high temperature and conductor resistance calculations showed that at conductor temperatures above $140\text{ }^\circ\text{C}$, the linear relationship between the temperature and resistance becomes extremely erroneous. Above $140\text{ }^\circ\text{C}$, the conductor resistivity ought to be determined by second order curves, presented in equation (4.1) [68].

$$\rho = \rho_{20} \left[1 + \alpha_{20}(T_{av} + 20) + \zeta_{20}(T_{av} + 20)^2 \right] \quad (4.1)$$

ρ_{20} = conductor resistivity at $20\text{ }^\circ\text{C}$

α_{20} and ζ_{20} are the linear & quadratic temperature coefficients, respectively.

The IEEE and the CIGRÉ methods do not include the quadratic term in the resistance expressions. This could result in excessive errors in the ampacity calculations because the models underestimate the conductor resistance calculations.

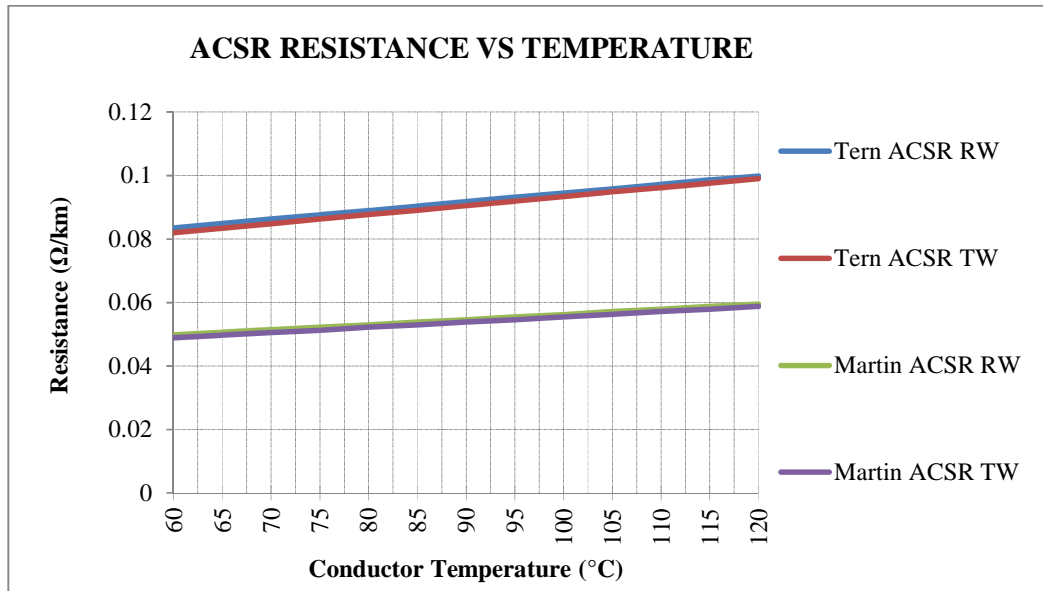


Figure 4-11: ACSR TW and RW Conductors' Resistance to Temperature Relationships

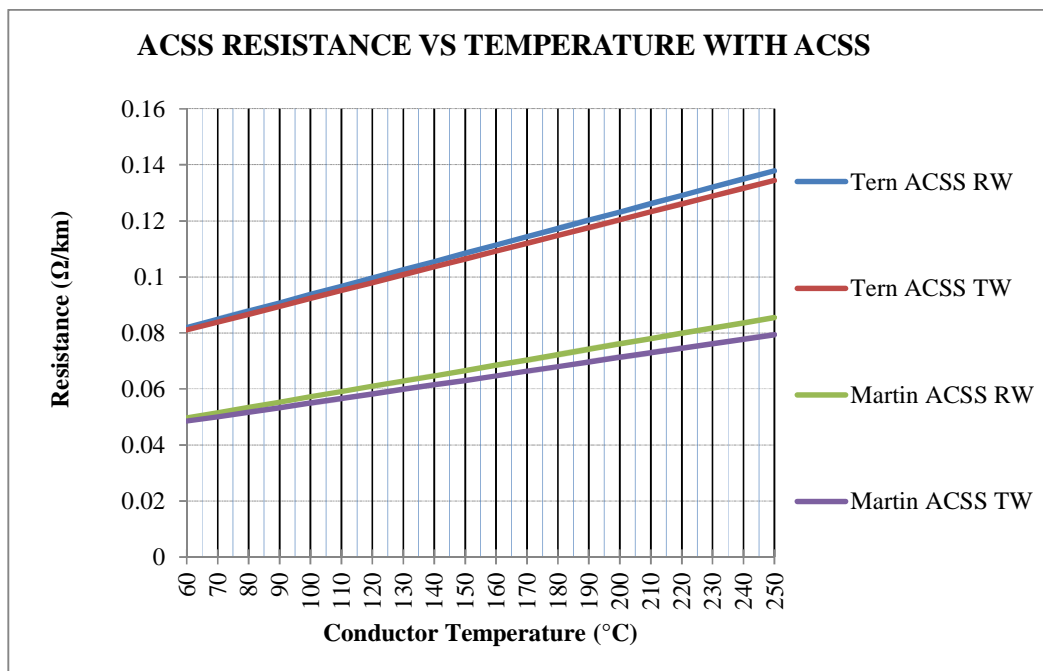


Figure 4-12: ACSS TW and RW Conductors' Resistance to Temperature Relationships

4.4 TW and RW Ampacity Comparisons

This section presents the ampacity comparisons of the conductors in TW and RW shapes using the CIGRÉ method. It was shown from the previous results, where the CIGRÉ and the IEEE methods were compared that the CIGRÉ method was more conservative. Moreover, the CIGRÉ method does not differentiate between the industrial and clear weather conditions, but it populates the results regardless of whether the environment is industrial or rural. Hence, the CIGRÉ method is appropriate for this general study which seeks to compare the performances of the conductors.

The same assumptions presented in Table 4-1 are used for the ampacity comparisons of the RW and TW conductors in ACSR and ACSS types of different diameters: Tern and Martin. Figure 4-13 and Figure 4-14 show the graphs relating the ampacity and the temperature of the ACSR conductors and ACSS conductors, respectively for the studied conductors.

At conductor temperatures below 55 °C, unanticipated results are observed. Firstly, at conductor temperatures of 50 °C and below, the ampacities of the conductors were zeros. This was because the conductor temperatures of 50 °C and below are very close to the ambient temperatures and the heat energy components result to zero. Most of the heat energy components in the heat balance equation are dependent on the average temperature presented as equation (2.5). Secondly, the results show that Tern conductor has larger ampacity values at the conductor temperatures of 50 °C and below than the results obtained with the use of Martin conductor. It is not expected that Tern conductor, which has a smaller diameter than that of Martin, could have larger ampacity values when compared to Martin conductor. Hence, Figure 4-13 and Figure 4-14 established that the heat balance equation according to the CIGRÉ method, cannot produce usable results at conductor temperatures below 50 °C and inclusive.

At conductor temperatures of 60 °C and above, the results are practical in that the expected pattern is observed where the larger conductors in diameter have higher values of ampacity than smaller diameter conductors. Figure 4-13 shows a marginal difference in the ampacity between RW to TW of ACSR conductors. The differences for Tern ACSR conductor range between 0.9 % at 65 °C, 2.0 % at 100 °C and 2.36 % at 120 °C. For Martin ACSR conductor, the differences are within 0.4 %, 1.73 % and 1.94 % at conductor temperatures of 65 °C, 100 °C and 120 °C, respectively. Comparisons of ACSS conductors as shown in Figure 4-14, portray the variances with Tern conductor as 0.44 %, 1.89 % and 2 % at conductor temperatures of 60 °C, 100 °C and 250 °C, correspondingly. Martin conductor showed differences in the range of 0.67 % at 60 °C, 0.46 % at 100 °C and 0.69 % at 250 °C.

The ampacity differences of TW and RW for the ACSR conductors consistently increase with the increase in the conductor temperature as expected. A similar pattern is observed in Tern ACSS conductors. However, with Martin conductor unexpected results are observed, where the differences fluctuate inconsistently with the increase in temperature. The slight differences in ampacity observed between the TW and RW conductors are attributable to the small variations of the resistances and the dissimilarities in their diameters. As illustrated in Table 3-1, the diameter differences between Tern TW and RW is 10% and 8.7 % for Martin conductor. Also the differences in resistances as presented in Figure 4-11 and Figure 4-12 influence the ampacity results through the heat balance equation.

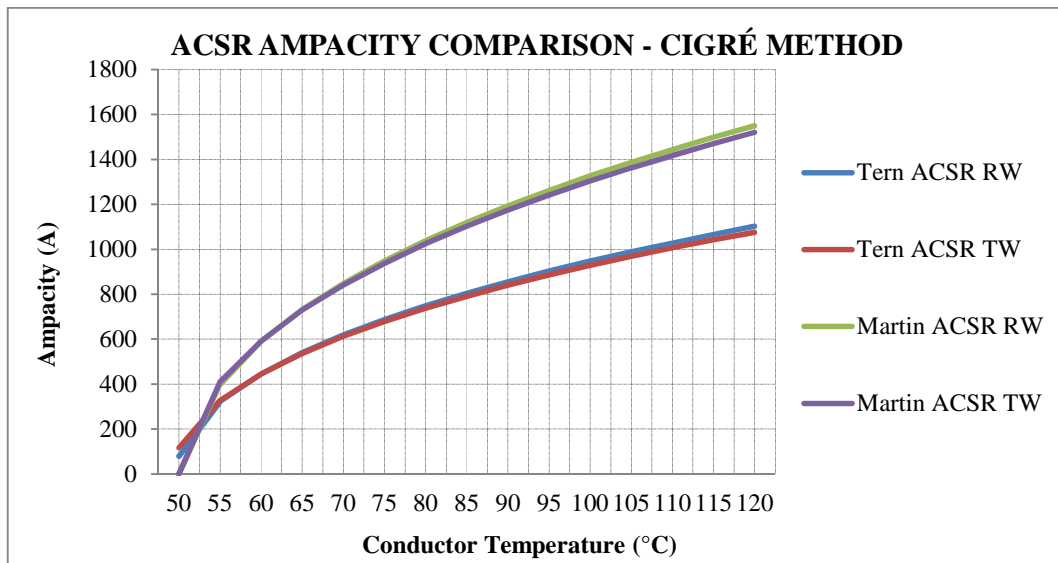


Figure 4-13: Ampacity plots of ACSR conductors in TW and RW forms of different diameters

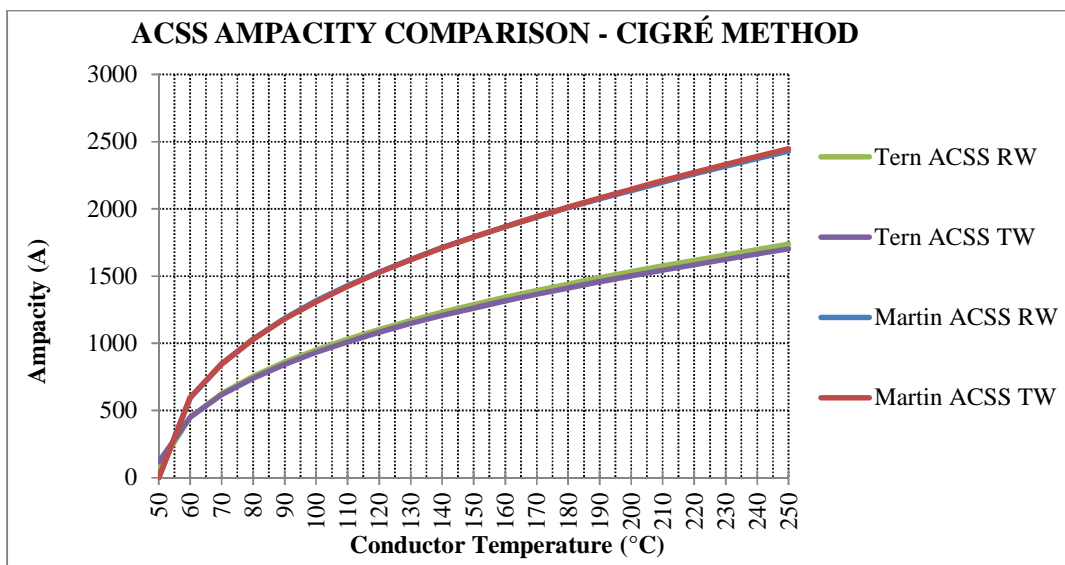


Figure 4-14: Ampacity plots of ACSS conductors in TW and RW forms of different diameters

Figure 4-15 compares the ampacity and conductor temperature relationships of ACSR and ACSS conductors in RW shapes. The graphs show that the ACSR and ACSS conductors have the same current-temperature profiles except that the ACSS conductors can produce results at temperatures above the conventional 100 °C. This demonstrates that if the ACSS conductor is operated at temperatures below 100 °C, it yields the ampacity values which are the same as the values from ACSR conductor. The results also prove that the ACSS conductor is similar to ACSR conductor, the difference is only in the ability of the ACSS conductor to be operated at high temperatures. Hence, ACSS conductors can be installed in new lines where there are right-of-way restrictions so that the transmission line can be thermally uprated at a later stage, without the re-acquisition of land.

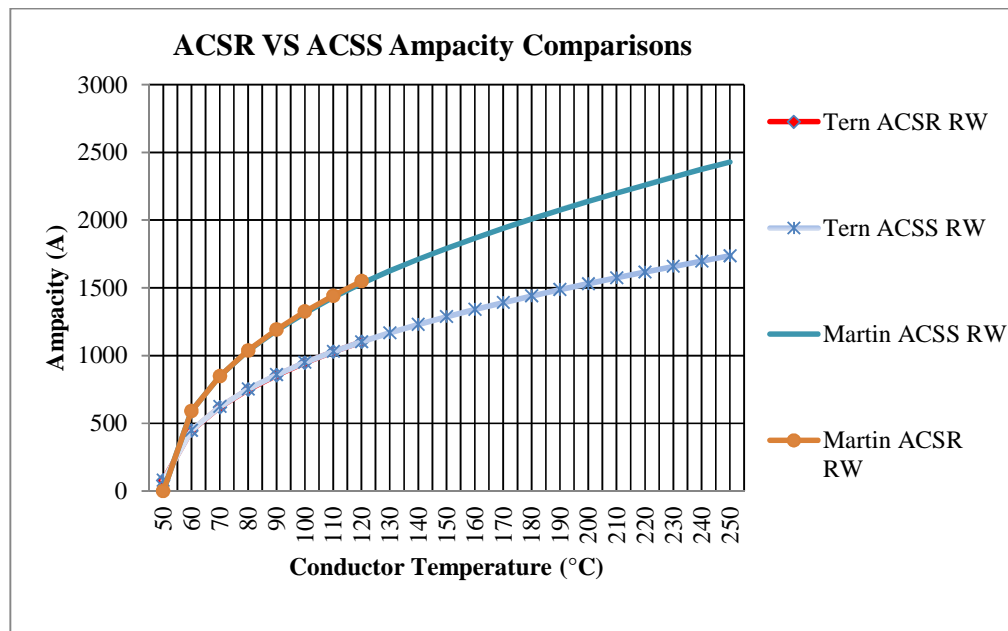


Figure 4-15: Ampacity plots of ACSR and ACSS conductors in RW forms

4.5 Power Losses Comparisons

The ohmic power losses as functions of the conductor temperatures of Tern and Martin conductors in ACSR and ACSS types of RW and TW forms are presented Figure 4-16 and Figure 4-17, respectively. As expected, the power losses increase with the increase in conductor temperature, due to the relationship, I^2R . Both the current and the resistance are temperature dependent variables. The losses are calculated per kilometer of the conductor length.

At conductor temperatures below 80 °C, the losses are less than 1 MW/km for ACSR conductors and at conductor temperatures of less than 90 °C for ACSS conductors. These

observations are attributable with the inconsistent ampacity values obtained at lower temperatures from the ampacity models.

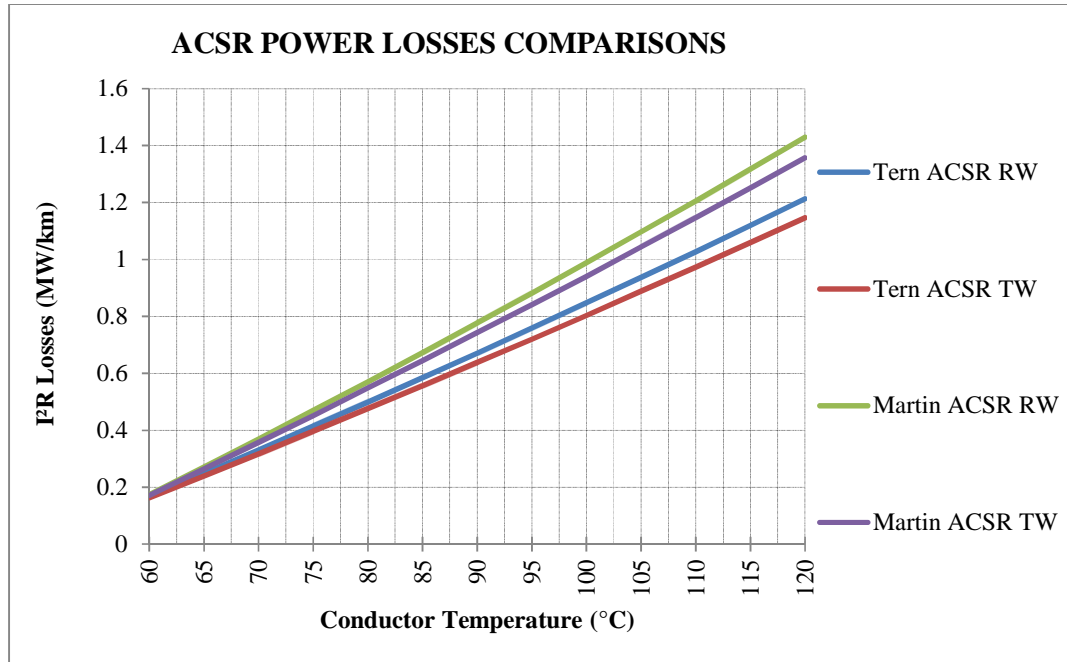


Figure 4-16: Power losses comparisons of ACSR conductors in TW and RW shapes

Significant differences between RW and TW are observed at temperatures above 80 °C in both ACSR and ACSS conductors. TW conductors have much less power losses compared to RW and the differences increase with temperature increase in both conductor types. The power loss differences between the RW and TW conductors in ACSR types range from 1.8 % to 5.5 % for Tern conductor and 1.1 % to 5.1 % for Martin at conductor temperatures of 60 °C to 120 °C as shown in Table 4-6. The percentage differences for RW and TW of ACSS conductor type are presented in Table 4-7.

Table 4-6: Percentage differences between RW and TW conductors of ACSR types

Conductor Temperature (°C)	% Difference of RW and TW Tern ACSR	% Difference of RW and TW Martin ACSR
60	1.80	1.14
65	3.57	2.58
70	3.95	3.37
75	4.33	3.99
80	4.59	3.96
85	4.84	4.11
90	4.74	4.42
95	5.19	4.55
100	5.19	4.81

Conductor Temperature (°C)	% Difference of RW and TW Tern ACSR	% Difference of RW and TW Martin ACSR
105	5.20	4.79
110	5.22	4.90
115	5.42	5.02
120	5.52	5.13

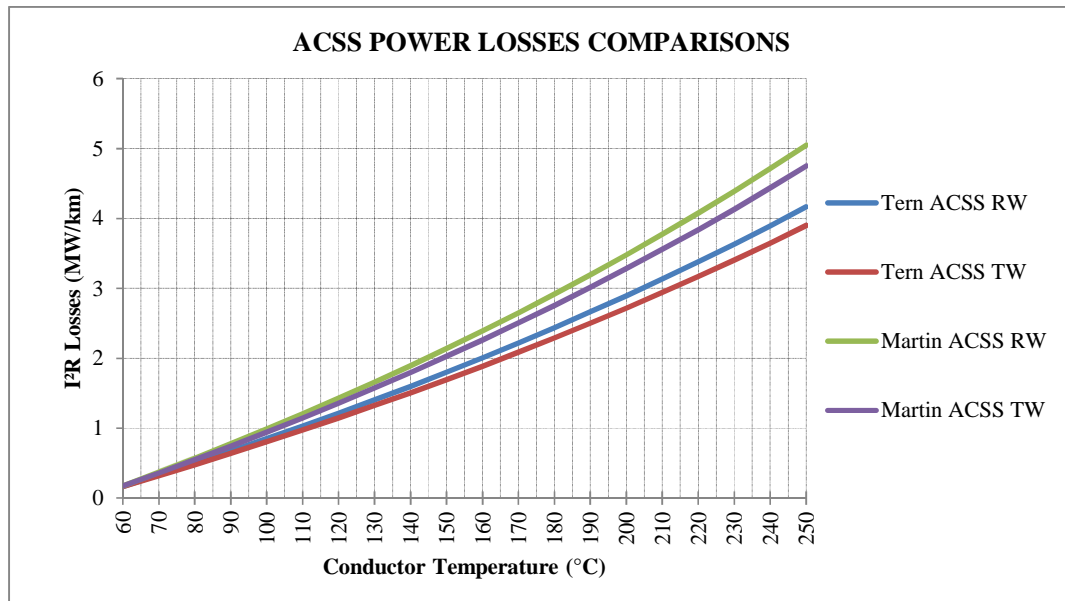


Figure 4-17: Power losses comparisons of ACSS conductors in TW and RW shapes

Table 4-7: Percentage differences between RW and TW conductors of ACSS types

Conductor Temperature (°C)	% Difference of RW and TW Tern ACSR	% Difference of RW and TW Martin ACSR
60	1.97	0.89
70	3.70	3.41
80	4.74	4.12
90	5.07	4.43
100	5.19	4.72
110	5.33	5.03
120	5.32	5.09
130	5.58	4.97
140	5.59	5.17
150	5.85	5.26
160	5.88	5.45
170	5.99	5.39
180	6.03	5.57
190	6.15	5.66
200	6.06	5.61
210	6.23	5.69

Conductor Temperature (°C)	% Difference of RW and TW Tern ACSS	% Difference of RW and TW Martin ACSS
220	6.27	5.77
230	6.38	5.81
240	6.31	5.84
250	6.35	5.83

It is depicted in the tables and the charts: Table 4-6 and Table 4-7; Figure 4-16 and Figure 4-17; that there are notable benefits of using TW conductors instead of their RW counterparts at temperatures above 80 °C for ACSR conductors and above 90 °C for ACSS conductors. This can be translated to the initial investment cost calculated from the total cost of losses as discussed in section 1.2.6. If the cost of TW conductor is known, then the cost of savings in using TW conductor instead of RW counterparts can be quantified.

ACSR and ACSS conductor power loss contrasts are consistent with the ampacity results, in that at conductor temperatures below 120 °C, precisely the same results were obtained for RW and TW counterparts. The ACSR and ACSS conductor equivalents have the same conductor resistances and diameters, which result in equal power losses at the same conductor temperatures.

The power loss comparisons of different conductor resistances i.e. Martin and Tern conductors show that Tern conductor has lower losses than Martin conductors at conductor temperatures above 80 °C and 90 °C for ACSR and ACSS, respectively. Below the 80 °C and 90 °C temperature zones, the expectation that conductors with different resistances and diameters result in different power losses is not recognizable. Although Martin conductor has a lower resistance than Tern conductors, which could mean lower losses, its larger diameter resulted to a larger ampacity than that of Tern conductor and hence more losses when compared to Tern conductor.

4.6 Magnetic Field Results

Magnetic fields were computed for ACSR and ACSS conductors along the right-of-way width of 55 m. The calculations were made from the centre to the edges of the right-of-way. The 520B structures of the third section of the PLS-CADD line model had the lowest mid-span. Hence the magnetic fields along the line servitude width were computed with reference to 520B structures. The phase-to-phase dimensions of the 520B structure are presented in Appendix B. Triple bundles were assumed for Martin conductors and quad bundles were assumed for Tern conductors. A sub-conductor spacing of 450 mm was used for both conductor types based on equation (3.8).

The magnetic fields of ACSR conductors were computed using the ampacity values obtained at the maximum conductor temperatures of 100 °C and 120 °C. The ampacity values at these temperatures are presented in Table 4-8.

Figure 4-18 and Figure 4-19 present the magnetic field results obtained from the ampacity values at 100 °C and 120 °C, respectively. At the conductor temperature of 100 °C, the maximum magnetic field value of 19.2 μT is observed with Martin conductor in RW form at the centre of the right-of-way. This is because Martin RW has the largest value of ampacity due to its larger diameter compared to the other conductors.

Table 4-8: Ampacity values used for magnetic field calculations of ACSR Conductors

Conductor Type	Ampacity (A)	
	Conductor Temperature (100 °C)	Conductor Temperature (120 °C)
Tern ACSR RW	947	1102
Tern ACSR TW	928	1076
Martin ACSR RW	1326	1550
Martin ACSRTW	1303	1520

Both graphs of Figure 4-18 and Figure 4-19 show that the magnetic field are well below the limits stipulated by ICNIP. The graphs also show that there are not much visible differences between the RW and TW conductor forms in ACSR type. The slight differences at the centre of the right-of-way between the two forms are mostly due to the differences in diameters and resistances. Additionally, the magnitudes of magnetic fields at the centre of the servitude are larger relative to the fields at the edge of the servitude. This is due to the additions of the fields from all three phases of the line and that the conductor phases are horizontally configured. A 2% difference is observed between Martin RW and TW conductors at the centre of the servitude.

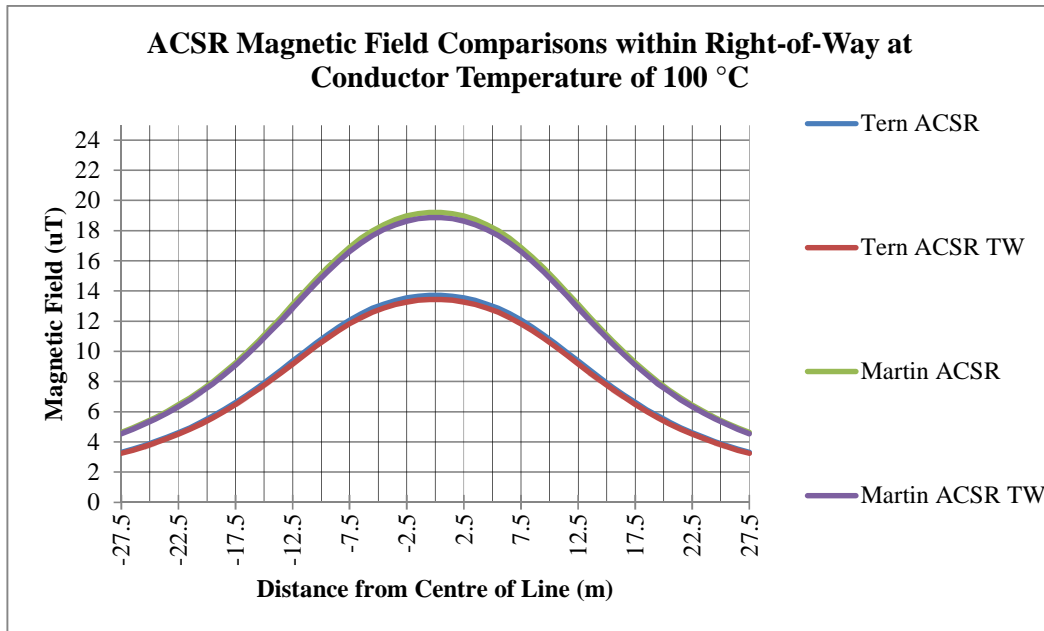


Figure 4-18: ACSR magnetic fields at conductor temperature of 100 °C

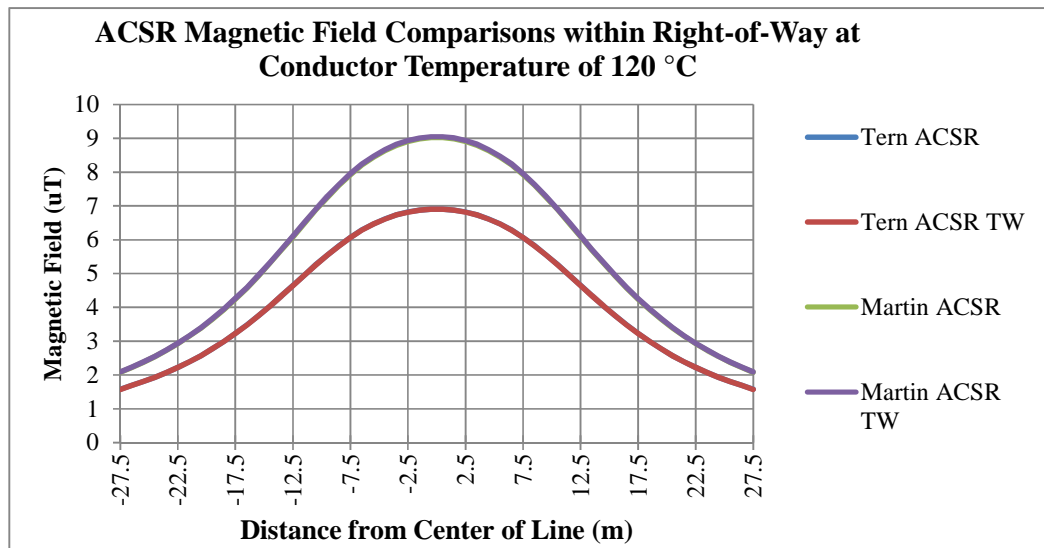


Figure 4-19: ACSR magnetic fields at conductor temperature of 120 °C

The magnetic fields for ACSS conductors were computed using the conductor temperatures, 190 °C and 250 °C. Table 4-9 presents the ampacity values used in the calculations of the magnetic fields. Figure 4-20 and Figure 4-21 show the magnetic field results for the ACSS conductors. Again, RW and TW conductors have similar magnetic field values. Martin conductor has the maximum magnetic field because of its maximum ampacity. The ampacity values are a function of conductor diameter and resistance.

Table 4-9: Ampacity values used for magnetic field calculations of ACSS Conductors

Conductor Type	Ampacity (A)	
	Conductor Temperature (100 °C)	Conductor Temperature (120 °C)
Tern ACSR RW	1488	1738
Tern ACSR TW	1458	1703
Martin ACSR RW	2075	2430
Martin ACSRTW	2081	2447

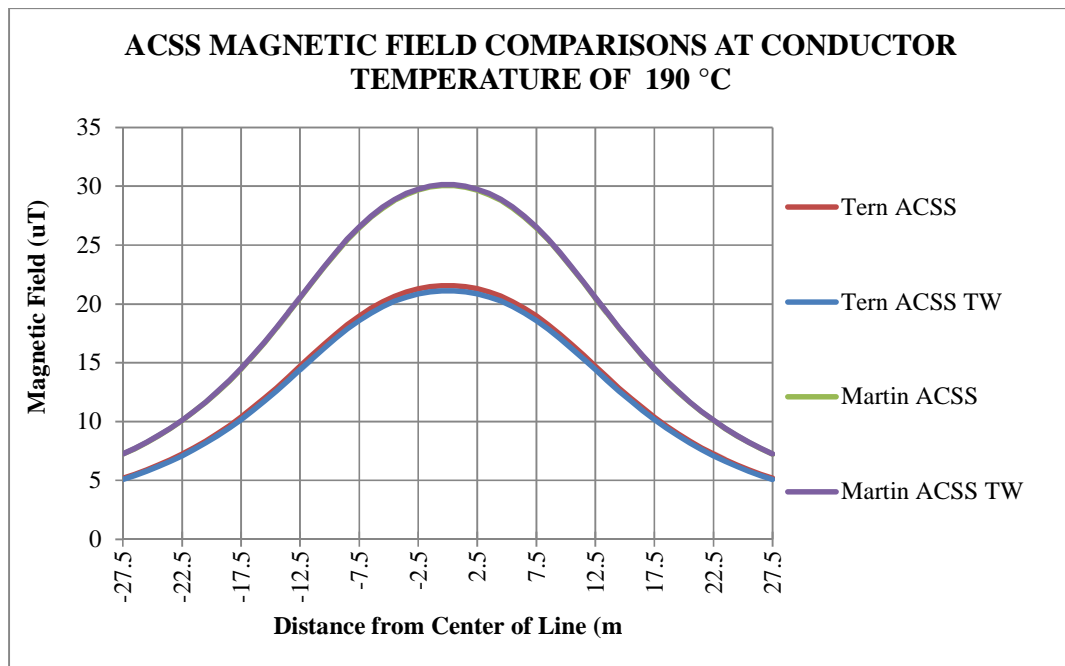


Figure 4-20: ACSS magnetic fields at conductor temperature of 250 °C

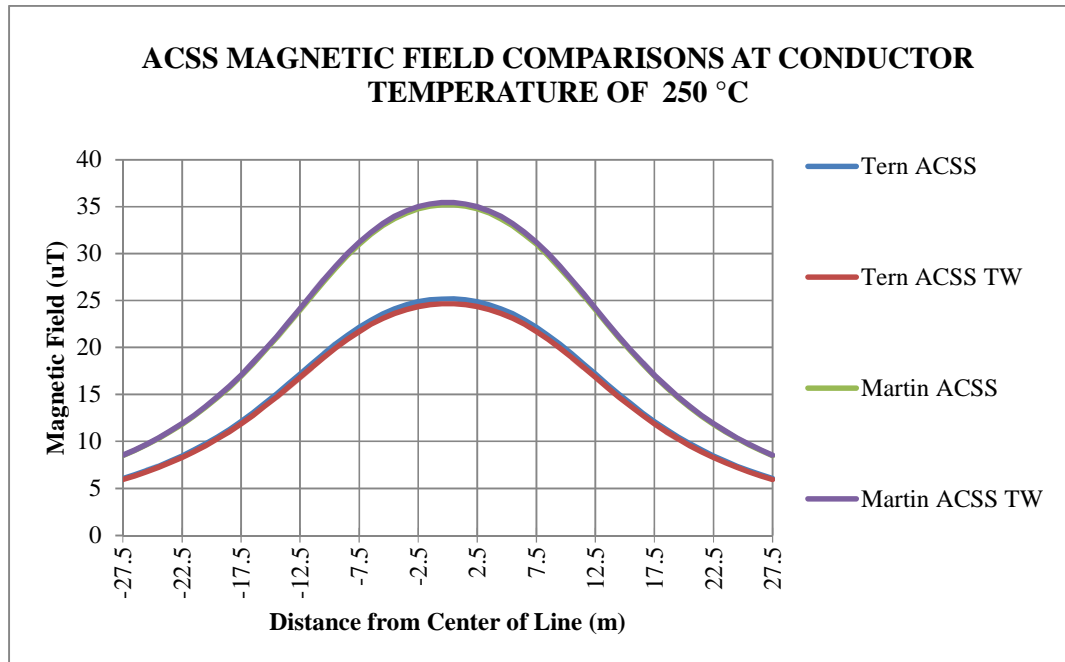


Figure 4-21: ACSS magnetic fields at conductor temperature of 250 °C

4.7 Summary

The comparisons of the IEEE and the CIGRÉ methods revealed differences in the calculations of solar heating, radiative cooling and AC resistance between the methods. The overall ampacity differences between the two methods resulted in about 2 %. In both methods, there was no certainty for the calculations of thermal ratings at temperatures above 100 °C. The CIGRÉ method was chosen to be used for the comparisons of the conductors because it populates general thermal ratings of the conductors for both industrial and clear environmental conditions.

There were no noteworthy differences in the current carrying capacities between TW and RW conductors in both ACSR and ACSS conductor types. The variances between TW and RW of ACSR type were in the order of 2 % for Tern conductor and 2.5 % for Martin conductor.

The ohmic power loss comparisons resulted in significant differences which were in the range of 5% at MCT for all the conductors, where TW conductors offered better benefits than RW conductors.

The magnetic field comparisons followed the trend of the ampacity comparisons with only a difference of 2 % observed between TW and RW conductors for Martin ACSS type. The RW conductor in this case had the largest value of magnetic fields. However, the magnetic field levels were below the stipulated ICNIP levels.

Chapter 5

CONCLUSIONS AND RECOMMENDATIONS

5.1 CONCLUSIONS

This study aimed at comparing the electrical performances of TW and RW of ACSR and ACSS conductor types used for overhead power transmission. The main objective was to determine and to quantify the benefits of using TW conductors as substitutes to RW counterparts for the purposes of re-conductoring an existing line or in stringing a new line. The electrical performances that were studied included thermal ratings, power losses, and magnetic fields. The electrical performance comparisons of the TW and RW forms in both ACSR and ACSS conductor types were evaluated. Two conductors of different diameters, Tern and Martin in their TW and RW forms were used in all the comparisons.

The IEEE and CIGRÉ methods were identified as the widely used methods for thermal ratings. The magnetic fields were computed using the EPRI method by modelling a real transmission line on PLS-CADD software. Ratekit version 5 computer program was used to evaluate the thermal rating of the conductors. Both IEEE and CIGRÉ methods are represented in the Ratekit program.

It was required that the models for evaluating thermal ratings of conductors be contrasted before calculations are made to determine the best method to be used for this particular study. The major differences between the two methods were observed in the solar heating results, convective cooling and the method of calculating the resistances. Solar heating calculations were different mainly because the CIGRÉ method considers both direct radiation and diffuse radiation, but do not include the angle of solar orientation to the conductor. Conversely, the IEEE method uses only the direct radiation and the atmospheric effects, clear or industrial, of the transmission line environment and also includes the orientation angle of sun with respect to the conductor. Furthermore, the input requirements for the two methods were different and that the IEEE method distinctly calculated urban and clear environmental based thermal ratings.

The application of the two thermal rating models at high temperatures could not be verified except for the fact that kinetic viscosity, air density and Prandtl numbers are calculated for temperatures of up to 100 °C in both methods. The IEEE method tabulated the kinetic viscosity and air density values for temperatures up to 100 °C. Furthermore, the AC resistances of both methods are calculated for temperatures below 100 °C [69]. Hence, there is no surety that these parameters can be used for high temperature calculations in both methods. Although there was

one study that validated the use of the thermal rating models at high temperature operations of the conductors [53], there is still some skepticism in using the models. The resistance-temperature relationship of the conductor has been proven not to be linear at temperatures above 100 °C. Nevertheless, there have been some suggestions that currently, a group of specialists at CIGRÉ are developing a thermal rating model that encompasses all the different characteristics of HTLS conductors [53].

For this study, the CIGRÉ model worked out to be the most efficient method for thermal rating evaluations because the comparisons between conductors were to be quantified. However, the differences between the two models were marginal. For the reason that in this study there was no need to differentiate between urban and rural environment, the CIGRÉ method was therefore used.

The contrasts between TW and RW conductor thermal ratings showed differences of about 2 %. The differences between the properties of TW and RW that have a direct impact on the ampacity calculations are the diameters and resistances. RW have diameters of about 10% larger than TW for Tern conductors and about 8.7% for Martin conductor, but the aluminium or conducting areas are the same. TW resistances are marginally lower than those of RW for both ACSR and ACSS conductors. The slight differences observed of less than 2 % in the electrical performances are due to the differences in the diameters and the minor inconsistencies in the resistances of the TW and RW shapes. The diameter influence to the electrical performance is clearly seen when Martin and Tern conductors are correlated.

This study has proven that conductors forged in TW shapes having different diameters from those in RW shapes provide marginal benefits when the ampacity and magnetic field performances are correlated. The physical shape of the conductor does not influence the electrical performance in terms of ampacity and magnetic fields, if the diameters and resistances are the same.

It can be concluded that the ampacity rating of an overhead transmission line is dependent upon the electrical parameters of the conductors, such as the resistance and the diameter of the conductor as opposed to the physical and metallurgical characteristics of the installed conductor. Conductor forging does not alter the electrical performance of the conductor if the conductor resistance and diameter is not altered. The alteration of the physical and metallurgical properties of the conductor may enhance the mechanical performance such as vibration and sagging properties, which were not studied in this project.

Significant benefits for using TW conductors could be derived from the ohmic power loss comparisons. Differences which were as high as 5 % were observed when comparing the ohmic power losses of TW and RW conductors. However, the cost of TW conductors and their relative initial investment and cost of savings due to the reduced cost of losses when compared to RW conductors were not evaluated to ascertain the cost benefit for using TW conductors.

5.2 RECOMMENDATIONS

One of the major questions that could not be answered in this study is the validity of the applicability of the IEEE and the CIGRÉ thermal rating models to HTLS conductors. The error of the assumption that the AC resistance assumes a linear dependency on temperature could not be justified in this study. It may be noted that operating a transmission line at its maximum conductor temperature for a long period of time could affect the conductor aging [70]; hence it is highly recommended that the ACSS conductor aging need to be evaluated [71]. ACSS conductors are suitable for application where high electrical load is encountered because of the ability to operate at high temperatures.

The cost of power losses associated with the application of ACSS at high temperatures compared with ACSR conductors and the application of ACSS conductors to very long lines is another study that could be of interest. Similar studies to the ones performed in this work need to be performed for TW conductors with similar diameters and different conducting areas as RW conductors to evaluate and compare their performances is required. These comparisons seem to offer more electrical performance benefits than the different diameters option, because of their large diameters and smaller resistances.

REFERENCES

- [1] V. Morgan, "Rating of bare overhead conductors for continuous currents," *PROC. IEE*, vol. 114, no. 10, pp. 1473-1482, 1967.
- [2] I. Makhkamova, P. Taylor, J. Bumby and K. Mahkamov, "CFD Analysis of the Thermal State of an Overhead line Conductor," School of Engineering, Durham University, Durham, UK.
- [3] I. Albizu, E. Fernandez, A. Mazon and J. Bengoechea, "Influence of the conductor temperature error on the overhead line ampacity monitoring systems," *IET Generation, Transmission & Distribution*, vol. 5, no. 4, p. 40–447, July 2010.
- [4] A. G. Expósito, J. R. Santos and P. C. Romero, "Planning and operational issues arising from the widespread use of HTLS conductors," *IEEE Transactions on Power Systems*, vol. 22, no. 4, pp. 1446-1455, 2007.
- [5] CIGRÉ, "CIGRÉ TB 244 Conductors for the uprating of overhead lines," CIGRÉ WG B2.12, 2004.
- [6] P. Couneson, J. Lamsoul, D. Delplanque, T. Capelle, M. Havaux, D. Guery and X. Delree, "Improving the performance of existing high-voltage overhead lines by using compact phase and ground conductors," in *22-209 CIGRÉ Session 1998*, Belgium, 1998.
- [7] I. Zamora, A. Mazon, P. Eguia, R. Criado, C. Alonso, J. Iglesias and J. Saenz, "High-temperature conductors: a solution in the uprating of overhead transmission lines," Porto, Portugal, 2001.
- [8] K. Kopsidas and S. M. Rowland, "A performance analysis of reconductoring an overhead line structure," *IEEE Transactions on Power Delivery*, vol. 24, no. 4, pp. 2248-2256, 2009.
- [9] P. Musilek, J. Heckenbergerova and M. I. Bhuiyan, "Spacial analysis of thermal aging of overhead transmission conductors," *IEEE Transactions on Power Delivery*, vol. 27, no. 3, p. 1196, 2012.
- [10] L. Ren, J. Xiuchen and S. Gehao, "Research for dynamic increasing transmission capacity," in *2008 International Conference on Condition Monitoring and Diagnosis*, Beijing, China,

References

- 2008.
- [11] S. D. Foss, S. H. Lin and R. A. Fernandes, "Dynamic thermal line ratings part I dynamic ampacity rating algorithm," *IEEE Transactions on Power Apparatus and Systems*, Vols. PAS-102, no. 6, pp. 1858-1864, June 1983.
- [12] ICNIRP, "Guidelines for limiting exposure to time-varying electric, magnetic, and electromagnetic fields (up to 300 GHz)," Health Physics Society, Oberschleissheim, 1997.
- [13] M. Abdel-Salam, H. Abdallah, M. El-Mohandes and H. El-Kishky, "Calculation of magnetic fields from electric power transmission lines," *Electric Power Systems Research*, no. 49, pp. 99-105, 1999.
- [14] Y. Ahmed and S. M. Rowland, "Modelling linesmen's potentials in proximity to overhead lines," *IEEE transactions on power delivery*, vol. 24, no. 4, pp. 2270-2275, October 2009.
- [15] B. Zemljarić, "Calculation of the connected magnetic and electric fields around an overhead-line tower for an estimation of their influence on maintenance personnel," *IEEE transactions on power delivery*, vol. 26, no. 1, pp. 467-474, 2011.
- [16] Southwire, *Bare overhead transmission conductors, selection and application*, Albuquerque, NM: IEEE TP&C Winter Meeting, 2006.
- [17] S. Karabay, "ACSS/TW aerial high-temperature bare conductors as a remedy for increasing transmission line capacity and determination of processing parameters for manufacturing," *Material and Design*, vol. 30, no. 3, pp. 816-825, 2009.
- [18] R. F. Thrash, "Transmission Conductors - A review of the design and selection criteria," Southwire Communications, 2003.
- [19] F. Thrash, "ACSS/TW - an improved high temperature conductor for upgrading existing lines or new construction," Southwire Company, Carrollton, 2001.
- [20] H. W. Adams, "Steel supported aluminum conductors (SSAC) for overhead transmission lines," *IEEE transactions on power apparatus and systems*, Vols. PAS-93, no. 5, pp. 1700-1705, September, 1974.
- [21] "Increased ratings of overhead transmission circuits using HTLS and compact designs,"

References

- 2012.
- [22] S. Manjang, Y. George and I. Kitta, "Analysis of power losses of the 150 kV transmission using pointing vector," in *IEEE conference on power engineering and renewable energy*, Bali, Indonesia, July 2012.
- [23] I. Osman, A. R. Mahbub, M. A. Rahman and A. Haque, "Benefits of optimal size conductor in transmission system," Dhaka, Bangladesh.
- [24] D. Dama, D. Muftic and R. Vajeth, "Conductor optimisation for overhead transmission lines," in *Inaugural IEEE PES 2005 Conference and Exposition Africa*, Durban, South Africa, July 2005.
- [25] V. Flipovic-Gledja, V. Morgan and R. Findlay, "A unified model for predicting the electrical, mechanical and thermal characteristics of stranded overhead-line conductors," in *Electrical and computer engineering*, Canada, 1994.
- [26] A. Silva and J. Bezerra, "Applicability and limitations of ampacity models for HTLS conductors," *Electric Power System Research*, no. 93, pp. 61-66, 2012.
- [27] S. Beryozkina, A. Sauhats and E. Vanzovichs, "Climate conditions impact on the permissible load current of the transmission line," in *IEEE Trondheim PowerTech*, Trondheim, 2011.
- [28] J. Fu, S. Abdelkader, J. D. Morrow and B. Fox, "Partial least squares modelling for dynamic overhead line ratings," in *IEEE Trondheim PowerTech*, Trondheim, 2011.
- [29] IEEE, "Calculating the current-temperature of bare overhead conductors IEEE Standard 738," IEEE, New York, 2006.
- [30] CIGRÉ, "Thermal behaviour of overhead conductors CIGRÉ 207, WG 22.12," CIGRÉ, 2002.
- [31] S. Abbott, S. Abdelkader, L. Bryans and D. Flynn, "Experimental validation and comparison of IEEE and CIGRÉ dynamic line models," in *UPEC2010*, 2010.
- [32] V. T. Morgan, "Effects of alternating and direct current, power frequency, temperature, and tension on the electrical parameters of ACSR conductors," *IEEE Transactions on Power*

References

- Delivery*, vol. 18, no. 3, pp. 859-866, 2003.
- [33] V. Morgan, "Electrical characteristics of steel-cored aluminium conductors," Australia, 1965.
- [34] D. Douglass and L. Kirkpatrick, "AC resistance of ACSR - magnetic and temperature effects," *IEEE Transactions on Power Apparatus and Systems*, Vols. PAS-104, no. 6, pp. 1578-1584, 1985.
- [35] V. Morgan and R. Findlay, "The effect of frequency on the resistance and internal inductance of bare ACSR conductors," *IEEE Transactions on Power Delivery*, vol. 6, no. 3, pp. 1319-1326, 1991.
- [36] V. Morgan, B. Zhang and R. Findlay, "Effects of temperature and tensile stress on the magnetic properties of a steel core from an ACSR conductor," *IEEE Transactions on Power Delivery*, vol. 11, no. 4, pp. 1907-1913, 1996.
- [37] V. Morgan, B. Zhang and R. Findlay, "Effect of magnetic induction in a steel-cored conductor on current distribution, resistance and power loss," *IEEE Transactions on Power Delivery*, vol. 12, no. 3, pp. 1299-1308, 1997.
- [38] V. T. Morgan, "The current distribution, resistance and internal inductance of linear power system conductors - a review of explicit equations," *IEEE Transaction on Power Delivery*, vol. 28, no. 3, pp. 1252-1262, 2013.
- [39] M. W. DAVIS, "A new thermal rating approach: the real time thermal rating system for strategic overhead conductor transmission lines part III steady state thermal rating program," *IEEE Transactions on Power Apparatus and Systems*, Vols. PAS-97, no. 2, pp. 444-455, 1978.
- [40] Eskom, "The planning, design and construction of overhead power lines," in *The planning, design and construction of overhead power lines*, Johannesburg, 2005, pp. 324-371.
- [41] T. Ringelband, M. Lange, M. Dietrich and H.-J. Haubrich, "Potential of improved wind integration by dynamic thermal rating of overhead lines," in *IEEE Bucharest Power Tech Conference*, Bucharest, Romani, 2009.
- [42] B. Adam, "Weather-based and conductor state measurement methods applied for dynamic

References

- line rating forecasting," in *The International Conference on Advanced Power System Automation and Protection*, Gdansk, Poland, 2011.
- [43] A. A. Rahim and I. Z. Abidin, "Verification of conductor temperature and time to thermal-overload calculations by experiments," in *International Conference on Energy and Environment*, Malacca, 2009.
- [44] P. Zhang, M. Shao, A. R. Leoni, D. H. Ramsay and M. Graham, "Determination of static thermal conductor rating using statistical analysis method," in *DRPT2008 6-9 April 2008 Nanjing China*, Nanjing, China, 2008.
- [45] CIGRÉ, "CIGRÉ TB 299 Guide for selection of weather parameters for bare overhead conductor ratings," CIGRÉ WG B2.12, 2006.
- [46] J. Reding, "A method for determining probability based allowable current ratings for BPA transmission lines," *IEEE Transactions on Power Delivery*, vol. 9, no. 1, pp. 153 - 161, 1994.
- [47] M. W. Davis, "A new thermal rating approach: The real time thermal rating system for strategic overhead conductor transmission lines part IV daily comparisons of real-time and conventional thermal ratings and establishment of typical annual weather models," *IEEE Transactions on Power Apparatus and Systems*, Vols. PAS-99, no. 6, pp. 2184-2192, 1980.
- [48] H. Wan, J. D. McCalley and V. Vittal, "Increasing thermal rating by risk analysis," *IEEE Transactions on Power Systems*, vol. 14, no. 3, pp. 815-128, August 1999.
- [49] C. Nascimento, J. Brito, G. E. Filho, G. E. Braga, G. Mdranda, A. Bracarense and S. Ueda, "The state of the art for increased overhead line ampacity utilizing new technologies and statistical criteria," in *IEEEIPES Transmission & Distribution Conference & Exposition*, Latin America, 2004.
- [50] K. Kopsida, S. M. Rowland and B. Boumeid, "A holistic method for conductor ampacity and sag computation on an OHL structure," *IEEE Transaction on Power Delivery*, vol. 27, no. 3, pp. 1047 - 1054, 2012.
- [51] S.-D. Lee, K.-Y. Shin, H.-J. Song, D.-I. Lee and B.-U. Min, "The sag and fatigue properties of STACIR/AW as a high temperature, low sag conductor," Korea, 2006.

References

- [52] R. Geary, T. Condon, T. Kavanagh, O. Armstrong and J. Doyle, "Introduction of high temperature low sag conductors to the Irish transmission grid," in *CIGRE B2-104*, Paris, 2012.
- [53] D. Douglass, "A practical application of high temperature low sag (HTLS) conductors," 2010.
- [54] BPA, "Transmission efficiency initiative host demonstration project application of ACSR trapezoidal wire conductor for a 500-kV transmission line," EPRI, Pacific Northwest, 2011.
- [55] EPRI, EPRI transmission line reference book - 200 kV and above, third edition, Palo Alto, CA: Electric Power Research Institute, Inc, 2005.
- [56] F. Moro and R. Turri, "Fast analytical computation of power-line magnetic fields by complex vector method," *IEEE transactions on power delivery*, vol. 23, no. 2, pp. 1042-1048, 2008.
- [57] A. Mamishev, R. Nevels and B. Russell, "Effects of conductor sag on spatial distribution of power line magnetic field," *IEEE transactions on power delivery*, vol. 11, no. 3, pp. 1571-1576, 1996.
- [58] R. G. Olsen, D. Deno, R. S. Baishiki, J. R. Abbott, R. Conti, M. Frazier, K. JafTa, G. B. Niles, J. R. Stewart, P. Wong and R. M. ZaVadil, "Magnetic fields from electric power lines theory and comparison to measurements," *IEEE transactions on power delivery*, vol. 3, no. 4, pp. 2127-2136, 1988.
- [59] P. Cruz, A. de la Villa-Ja'en, A. G'omez-Exp'osito and J. A. P'erez, "Uncertainty assessment and validation of current remote measurement on high voltage overhead conductors," in *International Conference on Power Engineering, Energy and Electrical Drives*, Torremolinos (M'álaga), Spain., May 2011.
- [60] R. G. Olsen, S. D. Schennum and V. L. Chartier, "Comparisons of several methods for electromagnetic interference levels and calibration with long data," *IEEE Transactions on Power Delivery*, vol. 7, no. 2, pp. 903-913, April 1992.
- [61] S. P. Maruvada and V. L. Chartier, "Chapter 7: Corona and Field Effects," in *EPRI Transmission Line Reference Book—115-230 kV Compact Line Design*, Palo Alto,

References

- California, Electric Power Research Institute, Inc., 2005, pp. 7-1 - 7-42.
- [62] L. P. Luhlanga, R. Singh, O. Fourie, A. Burger, K. Ramharak, R. Ngozo, M. Harrison and S. Dubazana, "Verwoerdburg turn-ins (from Apollo- Pluto 400 kV line): final report," Eskom, LES, Johannesburg, 2011.
- [63] D. Douglass, "Sag-tension Calculations," in *IEEE TP&C Tutorial*, June, 2005.
- [64] I. 6. Standard, "Design criteria of overhead transmission lines," IEC, Geneva, 2007.
- [65] S. 10280, "South african national standard - SANS 10280-1:2013," 2013.
- [66] R. k. Varanasi and D. Martin, "DWTS Task 2, Potential transmission technologies to increase power transfers," ABB Inc. Electric Systems Consulting, Raleigh, NC, 19 October 2005.
- [67] S. Chen, W. Black and H. Loard, "High-temperature ampacity model for overhead conductors," *IEEE Transactions on Power Delivery*, vol. 17, no. 4, pp. 1136 - 1141, 2002.
- [68] CIGRÉ, "CIGRÉ TB 345 Alternating current (AC) resistance of helically stranded conductors," CIGRÉ B2.12, 2008.
- [69] N. Schmidt, "Comparisons between I.E.E.E AND CIGRÉ ampacity standards," *IEEE Transaction on Power Delivery*, vol. 14, no. 4, pp. 1555 - 1562, 1999.
- [70] F. Jakl and A. Jakl, "Effects of elevated temperatures on mechanical properties of overhead conductors under steady state short circuit conditions," *IEEE Transactions on Power Delivery*, vol. 15, no. 1, pp. 242-246, 2000.
- [71] V. Morgan, "Effect of elevated temperature operation on the tensile strength of overhead conductors," *IEEE Transactions on Power Delivery*, vol. 11, no. 1, pp. 345-352, 1996.

Appendices

Appendix A

Cable Data

Cable Model

- Nonlinear cable model (separate polynomials for initial and creep behavior for inner and outer materials)
- Linear elastic with permanent stretch due to creep proportional to creep weather case tension
- Linear elastic with permanent stretch due to creep specified as a user input temperature increase

Name: c:\users\212581523\documents\plscadd\conductors\tern_acsr.wir

Description: 795 kcmil 45/7 Strands TERN ACSR - Adapted from 1970's Publicly Available Data

Stock Number: tern_acsr

Cross section area (mm²): 430.58 Unit weight (N/m): 13.0732 Number of independent wires (1 unless messenger supporting other wires with a spacer): 1

Outside diameter (mm): 27.0002 Ultimate tension (N): 98305.7

Conductor is a J-Power Systems GAP type conductor strung with core supporting all tension.

Temperature at which strand data below obtained (deg C): 22.2222 Display Color: ■

Outer Strands

Final modulus of elasticity (see note below) (MPa/100): 517.106

Thermal expansion coeff. (/100 deg): 0.002304

Polynomial coefficients (all strains in %, stresses in MPa, see note)

	a0	a1	a2	a3	a4
Stress-strain	-10.172E	605.699	-1066.7	951.978	-321.34E
Creep	-0.3144	178.905	192.889	-792.71E	603.028

Note: Final modulus, stress-strain and creep are actual material values multiplied by ratio of outer strand area to total area.

Bimetallic Conductor Model...

Aluminum has a larger thermal expansion coefficient than steel. If Aluminum is used as the outer material over a steel core there is a temperature transition point at which the aluminum is no longer under tension.

Select the behavior you want for temperatures above the transition point

- Use behavior from Criteria/Bimetallic Conductor Model
- Aluminum does not take compression at high temperature (Bird Cage)
- Aluminum can go into compression at high temperature

Thermal Rating Properties

Resistance at two different temperatures

Resistance (Ohm/km) 0.0736325 at (deg C) 25

Resistance (Ohm/km) 0.088359 at (deg C) 75

Emissivity coefficient: 0.5

Solar absorption coefficient: 0.5

Outer strands heat capacity (Watt-s/m-deg C): 1063.48

Core heat capacity (Watt-s/m-deg C): 103.535

Core Strands (if different from outer strands)

Final modulus of elasticity (see note below) (MPa/100): 124.795

Thermal expansion coeff. (/100 deg): 0.001152

Polynomial coefficients (all strains in %, stresses in MPa, see note)

	b0	b1	b2	b3	b4
Stress-strain	0.11859	116.177	7.02781	10.7903	-78.834E
Creep	0.11859	116.177	7.02781	10.7903	-78.834E

Note: Final modulus, stress-strain and creep are actual material values multiplied by ratio of core strand area to total area.

Maximum initial compressive stress (MPa): 68947.4

Buttons: Generate Coefficients for outer strands from points on stress-strain or creep curves, Graph Cable Properties, Generate Coefficients for core strands from points on stress-strain or creep curves, Composite cable properties, OK, Cancel

Figure A 1: PLS-CADD conductor file for Tern ACSR conductor in RW form

Cable Data

Cable Model

Nonlinear cable model (separate polynomials for initial and creep behavior for inner and outer materials)

Linear elastic with permanent stretch due to creep proportional to creep weather case tension

Linear elastic with permanent stretch due to creep specified as a user input temperature increase

Name: c:\users\2j2561623\documents\plscadd\conductors\tern_acsr_tw.wir

Description: 795 kcmil Type 7 TERN-TW ACSR TW - Adapted from 1970's Publicly Available Data

Stock Number: tern-tw_acsr_tw

Cross section area (mm²): 430.644 Unit weight (N/m): 13.0542 Number of independent wires (1 unless messenger supporting other wires with a spacer): 1

Outside diameter (mm): 24.3078 Ultimate tension (N): 96971.2

Conductor is a J-Power Systems GAP type conductor strung with core supporting all tension.

Temperature at which strand data below obtained (deg C): 22.2222 Display Color:

Outer Strands					Core Strands (if different from outer strands)						
Final modulus of elasticity (see note below)	(MPa/100)				517.106	Final modulus of elasticity (see note below)	(MPa/100)				124.795
Thermal expansion coeff.	(/100 deg)				0.002304	Thermal expansion coeff.	(/100 deg)				0.001152
Polynomial coefficients (all strains in %, stresses in MPa, see note)											
Stress-strain	a0	a1	a2	a3	a4	Stress-strain	b0	b1	b2	b3	b4
	-10.172E	605.699	-1066.7	951.978	-321.34E		0.11859	116.177	7.02781	10.7903	-78.834E
Creep	c0	c1	c2	c3	c4	Creep	d0	d1	d2	d3	d4
	-0.3144	178.905	192.889	-792.71E	603.028		0.11859	116.177	7.02781	10.7903	-78.834E

Note: Final modulus, stress-strain and creep are actual material values multiplied by ratio of outer strand area to total area.

Note: Final modulus, stress-strain and creep are actual material values multiplied by ratio of core strand area to total area.

Bimetallic Conductor Model..

Aluminum has a larger thermal expansion coefficient than steel. If Aluminum is used as the outer material over a steel core there is a temperature transition point at which the aluminum is no longer under tension.

Select the behavior you want for temperatures above the transition point

Use behavior from Criteria/Bimetallic Conductor Model

Aluminum does not take compression at high temperature (Bird Cage)

Aluminum can go into compression at high temperature

Maximum (value) compressive stress (MPa): 60347.4

Thermal Rating Properties

Resistance at two different temperatures

Resistance (Ohm/km) 0.0721 at (deg C) 25

Resistance (Ohm/km) 0.0863 at (deg C) 75

Emissivity coefficient: 0.5

Solar absorption coefficient: 0.5

Outer strands heat capacity (Watt-s/m-deg C):

Core heat capacity (Watt-s/m-deg C):

Buttons: Generate Coefficients for outer strands from points on stress-strain or creep curves, Graph Cable Properties, Generate Coefficients for core strands from points on stress-strain or creep curves, Composite cable properties, OK, Cancel

Figure A 2: PLS-CADD conductor file for Tern ACSR conductor in TW form

Appendices: Appendix A

Cable Data

Cable Model

Nonlinear cable model (separate polynomials for initial and creep behavior for inner and outer materials)

Linear elastic with permanent stretch due to creep proportional to creep weather case tension

Linear elastic with permanent stretch due to creep specified as a user input temperature increase

Name:

Description:

Stock Number:

Cross section area (mm ²)	<input type="text" value="430.58"/>	Unit weight (N/m)	<input type="text" value="13.0615"/>	Number of independent wires (1 unless messenger supporting other wires with a spacer)	<input type="text" value="1"/>
Outside diameter (mm)	<input type="text" value="27.0002"/>	Ultimate tension (N)	<input type="text" value="63164.7"/>	<input type="checkbox"/> Conductor is a J-Power Systems GAP type conductor strung with core supporting all tension.	

Temperature at which strand data below obtained (deg C) Display Color:

Outer Strands

Final modulus of elasticity (see note below) (MPa/100)

Thermal expansion coeff. (/100 deg)

Polynomial coefficients (all strains in %, stresses in MPa, see note)					
a0	a1	a2	a3	a4	
Stress-strain	1.16521	361.298	-1361.02	2405.99	-1570.3E
	c0	c1	c2	c3	c4
Creep	1.16521	361.298	-1361.02	2405.99	-1570.3E

Note: Final modulus, stress-strain and creep are actual material values multiplied by ratio of outer strand area to total area.

Core Strands (if different from outer strands)

Final modulus of elasticity (see note below) (MPa/100)

Thermal expansion coeff. (/100 deg)

Polynomial coefficients (all strains in %, stresses in MPa, see note)					
b0	b1	b2	b3	b4	
Stress-strain	-0.07101	125.864	-49.3664	80.6685	-89.355E
	d0	d1	d2	d3	d4
Creep	-0.07101	125.864	-49.3664	80.6685	-89.355E

Note: Final modulus, stress-strain and creep are actual material values multiplied by ratio of core strand area to total area.

Bimetallic Conductor Model..

Aluminum has a larger thermal expansion coefficient than steel. If Aluminum is used as the outer material over a steel core there is a temperature transition point at which the aluminum is no longer under tension.

Select the behavior you want for temperatures above the transition point

Use behavior from Criteria/Bimetallic Conductor Model

Aluminum does not take compression at high temperature (Bird Cage)

Aluminum can go into compression at high temperature

$\frac{V_{total} \text{ Stress} = A_{outer} \text{ Stress} + A_{in} \text{ Stress}}{A_{total}}$
 A_{in} = cross-section area of (circular) strands
 A_{total} = total cross-section area of entire conductor (outer + inner strands)

Maximum initial compressive stress (MPa)

Thermal Rating Properties

Resistance at two different temperatures

Resistance (Ohm/km) at (deg C)

Resistance (Ohm/km) at (deg C)

Emissivity coefficient

Solar absorption coefficient

Outer strands heat capacity (Watt-s/m-deg C)

Core heat capacity (Watt-s/m-deg C)

Generate Coefficients for outer strands from points on stress-strain or creep curves

Generate Coefficients for core strands from points on stress-strain or creep curves

Graph Cable Properties

Composite cable properties

Figure A 3: PLS-CADD conductor file for Tern ACSS conductor in RW form

Cable Data

Cable Model

Nonlinear cable model (separate polynomials for initial and creep behavior for inner and outer materials)

Linear elastic with permanent stretch due to creep proportional to creep weather case tension

Linear elastic with permanent stretch due to creep specified as a user input temperature increase

Name: c:\users\212551623\documents\plscadd\conductors\Tern_acss_tw.wtl

Description: 795.0 kcmil Type 7 ACSS "Tern/ACSS/TW" - Data herein is to be considered confidential and proprietary to Southwire and is for

Stock Number:

Cross section area (mm²) 430.644 Unit weight (N/m) 13.0032 Number of independent wires (1 unless messenger supporting other wires with a spacer) 1

Outside diameter (mm) 24.384 Ultimate tension (N) 63164.7

Conductor is a J-Power Systems GAP type conductor strung with core supporting all tension.

Temperature at which strand data below obtained (deg C) 21.1111 Display Color:

Outer Strands

Final modulus of elasticity (see note below) (MPa/100) 521.415

Thermal expansion coeff. (/100 deg) 0.002304

Polynomial coefficients (all strains in %, stresses in MPa, see note)

	a0	a1	a2	a3	a4
Stress-strain	1.16521	361.298	-1361.02	2405.99	-1570.3E
Creep	1.16521	361.298	-1361.02	2405.99	-1570.3E

Note: Final modulus, stress-strain and creep are actual material values multiplied by ratio of outer strand area to total area.

Core Strands (if different from outer strands)

Final modulus of elasticity (see note below) (MPa/100) 123.244

Thermal expansion coeff. (/100 deg) 0.001152

Polynomial coefficients (all strains in %, stresses in MPa, see note)

	b0	b1	b2	b3	b4
Stress-strain	-0.07101	125.864	-49.3664	80.6685	-89.355E
Creep	-0.07101	125.864	-49.3664	80.6685	-89.355E

Note: Final modulus, stress-strain and creep are actual material values multiplied by ratio of core strand area to total area.

Bimetallic Conductor Model..

Aluminum has a larger thermal expansion coefficient than steel. If Aluminum is used as the outer material over a steel core there is a temperature transition point at which the aluminum is no longer under tension.

Select the behavior you want for temperatures above the transition point

Use behavior from Criteria/Bimetallic Conductor Model

Aluminum does not take compression at high temperature (Bird Cage)

Aluminum can go into compression at high temperature

$W_{max}(\text{Stress}) = \frac{A_{out}(\text{Stress}) \cdot A_{in}}{A_{total}}$
 A_{out} = cross section area of outer strands
 A_{in} = total cross section area of inner conductor (outer + inner strands)

Maximum initial compressive stress (MPa) 68947.4

Thermal Rating Properties

Resistance at two different temperatures

Resistance (Ohm/km) 0.0712713 at (deg C) 25

Resistance (Ohm/km) 0.134838 at (deg C) 250

Emissivity coefficient 0.5

Solar absorption coefficient 0.5

Outer strands heat capacity (Watt-s/m-deg C) 1021.65

Core heat capacity (Watt-s/m-deg C) 100.394

Buttons: Generate Coefficients for outer strands from points on stress-strain or creep curves, Graph Cable Properties, Generate Coefficients for core strands from points on stress-strain or creep curves, Composite cable properties, OK, Cancel

Figure A 4: PLS-CADD conductor file for Tern ACSS conductor in TW form

Cable Data

Cable Model

Nonlinear cable model (separate polynomials for initial and creep behavior for inner and outer materials)

Linear elastic with permanent stretch due to creep proportional to creep weather case tension

Linear elastic with permanent stretch due to creep specified as a user input temperature increase

Name: c:\users\212561623\desktop\conductors\vmartin_acsr.wir

Description: 1351.5 kcmil 54/19 Strands MARTIN ACSR - Adapted from 1970's Publicly Available Data

Stock Number: martin_acsr

Cross section area (mm²): 771.611 Unit weight (N/m): 25.3496 Number of independent wires (1 unless messenger supporting other wires with a spacer): 1

Outside diameter (mm): 36.1696 Ultimate tension (N): 205953

Conductor is a J-Power Systems GAP type conductor strung with core supporting all tension.

Temperature at which strand data below obtained (deg C): 24.4444 Display Color:

Outer Strands						Core Strands (if different from outer strands)					
Final modulus of elasticity (see note below) (MPa/100): 490.906						Final modulus of elasticity (see note below) (MPa/100): 215.806					
Thermal expansion coeff. (/100 deg): 0.002304						Thermal expansion coeff. (/100 deg): 0.001152					
Polynomial coefficients (all strains in %, stresses in MPa, see note)						Polynomial coefficients (all strains in %, stresses in MPa, see note)					
a0 a1 a2 a3 a4						b0 b1 b2 b3 b4					
Stress-strain: -6.97817 460.195 -731.863 648.713 -234.042						Stress-strain: 2.60966 166.803 175.216 -399.764 190.633					
c0 c1 c2 c3 c4						d0 d1 d2 d3 d4					
Creep: 0.83564 151.918 -235.552 157.469 -17.4985						Creep: 2.60966 166.803 175.216 -399.764 190.633					

Note: Final modulus, stress-strain and creep are actual material values multiplied by ratio of outer strand area to total area.

Note: Final modulus, stress-strain and creep are actual material values multiplied by ratio of core strand area to total area.

Bimetallic Conductor Model..

Aluminum has a larger thermal expansion coefficient than steel. If Aluminum is used as the outer material over a steel core there is a temperature transition point at which the aluminum is no longer under tension.

Select the behavior you want for temperatures above the transition point

Use behavior from Criteria/Bimetallic Conductor Model

Aluminum does not take compression at high temperature (Bird Cage)

Aluminum can go into compression at high temperature

$\frac{Actual\ Stress}{Actual\ Stress} = \frac{A_c}{A}$

A_c = cross section area of outer strands

A = total cross section area of entire conductor (outer + inner strands)

Maximum initial compressive stress (MPa): 68847.4

Thermal Rating Properties

Resistance at two different temperatures

Resistance (Ohm/km): 0.0441174 at (deg C) 25

Resistance (Ohm/km): 0.0535622 at (deg C) 75

Emissivity coefficient: 0.5

Solar absorption coefficient: 0.5

Outer strands heat capacity (Watt-s/m-deg C): 3634.26

Core heat capacity (Watt-s/m-deg C): 646.157

Generate Coefficients for outer strands from points on stress-strain or creep curves

Graph Cable Properties

Generate Coefficients for core strands from points on stress-strain or creep curves

Composite cable properties

OK Cancel

Figure A 5: PLS-CADD conductor file for Martin ACSR conductor in RW form

Cable Data

Cable Model

Nonlinear cable model (separate polynomials for initial and creep behavior for inner and outer materials)

Linear elastic with permanent stretch due to creep proportional to creep weather case tension

Linear elastic with permanent stretch due to creep specified as a user input temperature increase

Name: c:\users\212561623\desktop\conductors\martin-tw_acsr_tw.wir

Description: 1351.5 kcmil Type 13 MARTIN-TW ACSR TW - Adapted from 1970's Publicly Available Data

Stock Number: martin-tw_acsr_tw

Cross section area (mm²): 771.611 Unit weight (N/m): 25.262 Number of independent wires (1 unless messenger supporting other wires with a spacer): 1

Outside diameter (mm): 32.9438 Ultimate tension (N): 208177

Conductor is a J-Power Systems GAP type conductor strung with core supporting all tension.

Temperature at which strand data below obtained (deg C): 24.4444 Display Color:

Outer Strands						Core Strands (if different from outer strands)																																									
Final modulus of elasticity (see note below) (MPa/100): 490.906						Final modulus of elasticity (see note below) (MPa/100): 215.806																																									
Thermal expansion coeff. (/100 deg): 0.002304						Thermal expansion coeff. (/100 deg): 0.001152																																									
Polynomial coefficients (all strains in %, stresses in MPa, see note)						Polynomial coefficients (all strains in %, stresses in MPa, see note)																																									
<table border="1"> <thead> <tr> <th></th> <th>a0</th> <th>a1</th> <th>a2</th> <th>a3</th> <th>a4</th> </tr> </thead> <tbody> <tr> <td>Stress-strain</td> <td>-6.97817</td> <td>460.195</td> <td>-731.865</td> <td>648.713</td> <td>-234.042</td> </tr> <tr> <td>Creep</td> <td>0.83564</td> <td>151.918</td> <td>-235.552</td> <td>157.469</td> <td>-17.4989</td> </tr> </tbody> </table>							a0	a1	a2	a3	a4	Stress-strain	-6.97817	460.195	-731.865	648.713	-234.042	Creep	0.83564	151.918	-235.552	157.469	-17.4989	<table border="1"> <thead> <tr> <th></th> <th>b0</th> <th>b1</th> <th>b2</th> <th>b3</th> <th>b4</th> </tr> </thead> <tbody> <tr> <td>Stress-strain</td> <td>2.60966</td> <td>166.803</td> <td>175.216</td> <td>-399.764</td> <td>190.633</td> </tr> <tr> <td>Creep</td> <td>2.60966</td> <td>166.803</td> <td>175.216</td> <td>-399.764</td> <td>190.633</td> </tr> </tbody> </table>							b0	b1	b2	b3	b4	Stress-strain	2.60966	166.803	175.216	-399.764	190.633	Creep	2.60966	166.803	175.216	-399.764	190.633
	a0	a1	a2	a3	a4																																										
Stress-strain	-6.97817	460.195	-731.865	648.713	-234.042																																										
Creep	0.83564	151.918	-235.552	157.469	-17.4989																																										
	b0	b1	b2	b3	b4																																										
Stress-strain	2.60966	166.803	175.216	-399.764	190.633																																										
Creep	2.60966	166.803	175.216	-399.764	190.633																																										

Note: Final modulus, stress-strain and creep are actual material values multiplied by ratio of outer strand area to total area.

Note: Final modulus, stress-strain and creep are actual material values multiplied by ratio of core strand area to total area.

Bimetallic Conductor Model..

Aluminum has a larger thermal expansion coefficient than steel. If Aluminum is used as the outer material over a steel core there is a temperature transition point at which the aluminum is no longer under tension.

Select the behavior you want for temperatures above the transition point

Use behavior from Criteria/Bimetallic Conductor Model

Aluminum does not take compression at high temperature (Bird Cage)

Aluminum can go into compression at high temperature

Thermal Rating Properties

Resistance at two different temperatures

Resistance (Ohm/km) _____ at (deg C) 25

Resistance (Ohm/km) _____ at (deg C) 75

Emissivity coefficient: 0.5

Solar absorption coefficient: 0.5

Outer strands heat capacity (Watt-s/m-deg C): _____

Core heat capacity (Watt-s/m-deg C): _____

Maximum initial compressive stress (MPa): 88347.4

Buttons: Generate Coefficients for outer strands from points on stress-strain or creep curves, Graph Cable Properties, Generate Coefficients for core strands from points on stress-strain or creep curves, Composite cable properties, OK, Cancel

Figure A 6: PLS-CADD conductor file for Martin ACSR conductor in TW form

Cable Data

Cable Model

- Nonlinear cable model (separate polynomials for initial and creep behavior for inner and outer materials)
- Linear elastic with permanent stretch due to creep proportional to creep weather case tension
- Linear elastic with permanent stretch due to creep specified as a user input temperature increase

Name: c:\users\212561623\documents\plsocadd\conductors\martin_acss.wir
 Description: 1351 kmil 54/19 Strands MARTIN ACSS - Data Provided by Southwire
 Stock Number: _____

Cross section area (mm²) 771.482 Unit weight (N/m) 25.319 Number of independent wires (1 unless messenger supporting other wires with a spacer) 1
 Outside diameter (mm) 36.1696 Ultimate tension (N) 161026

Conductor is a J-Power Systems GAP type conductor strung with core supporting all tension.

Temperature at which strand data below obtained (deg C) 21.1111 Display Color:

Outer Strands					Core Strands (if different from outer strands)						
Final modulus of elasticity (see note below)	(MPa/100) 484.011				Final modulus of elasticity (see note below)	(MPa/100) 212.358					
Thermal expansion coeff.	(1/100 deg) 0.002304				Thermal expansion coeff.	(1/100 deg) 0.001152					
Polynomial coefficients (all strains in %, stresses in MPa, see note)	a0	a1	a2	a3	a4	Polynomial coefficients (all strains in %, stresses in MPa, see note)	b0	b1	b2	b3	b4
Stress-strain	1.10674	343.138	-1292.5E	2285.06	-1491.61	Stress-strain	0.06715	197.3	-21.511E	-29.440E	-10.135E
	c0	c1	c2	c3	c4		d0	d1	d2	d3	d4
Creep	1.10674	343.138	-1292.5E	2285.06	-1491.61	Creep	0.06715	197.3	-21.511E	-29.440E	-10.135E

Note: Final modulus, stress-strain and creep are actual material values multiplied by ratio of outer strand area to total area. Note: Final modulus, stress-strain and creep are actual material values multiplied by ratio of core strand area to total area.

Bimetallic Conductor Model...
 Aluminum has a larger thermal expansion coefficient than steel. If Aluminum is used as the outer material over a steel core there is a temperature transition point at which the aluminum is no longer under tension.

Select the behavior you want for temperatures above the transition point

- Use behavior from Criteria/Bimetallic Conductor Model
- Aluminum does not take compression at high temperature (Bird Cage)
- Aluminum can go into compression at high temperature

Thermal Rating Properties

Resistance at two different temperatures:

Resistance (Ohm/km) 0.0429989 at (deg C) 25
 Resistance (Ohm/km) 0.0522573 at (deg C) 75

Emissivity coefficient: 0.5
 Solar absorption coefficient: 0.5
 Outer strands heat capacity (Watt-s/m-deg C) 1816.95
 Core heat capacity (Watt-s/m-deg C) 323.079

Maximum initial compressive stress (MPa) 58947.4

Buttons: Generate Coefficients for outer strands from points on stress-strain or creep curves, Graph Cable Properties, Generate Coefficients for core strands from points on stress-strain or creep curves, Composite cable properties, OK, Cancel

Figure A 7: PLS-CADD conductor file for Martin ACSS conductor in RW form

Cable Data

Cable Model

Nonlinear cable model (separate polynomials for initial and creep behavior for inner and outer materials)

Linear elastic with permanent stretch due to creep proportional to creep weather case tension

Linear elastic with permanent stretch due to creep specified as a user input temperature increase

Name: c:\users\212561623\documents\pls\cadd\conductors\martin_acss_tw.wir

Description: 1352 kcmil T13 (39/19) Martin ACSS TW - Data Provided by Southwire

Stock Number:

Cross section area (mm²): 771.547 Unit weight (N/m): 25.2752 Number of independent wires (1 unless messenger supporting other wires with a spacer): 1

Outside diameter (mm): 33.02 Ultimate tension (N): 161026

Conductor is a J-Power Systems GAP type conductor strung with core supporting all tension.

Temperature at which strand data below obtained (deg C): 21.1111 Display Color: ■

Outer Strands					Core Strands (if different from outer strands)						
Final modulus of elasticity (see note below)	(MPa/100)				484.011	Final modulus of elasticity (see note below)	(MPa/100)				212.358
Thermal expansion coeff.	(/100 deg)				0.002304	Thermal expansion coeff.	(/100 deg)				0.001152
Polynomial coefficients (all strains in %, stresses in MPa, see note)					Polynomial coefficients (all strains in %, stresses in MPa, see note)						
	a0	a1	a2	a3	a4	b0	b1	b2	b3	b4	
Stress-strain	1.10674	343.138	-1292.5E	2285.06	-1491.61	0.06715	197.3	-21.511E	-29.440E	-10.135E	
	c0	c1	c2	c3	c4	d0	d1	d2	d3	d4	
Creep	1.10674	343.138	-1292.5E	2285.06	-1491.61	0.06715	197.3	-21.511E	-29.440E	-10.135E	

Note: Final modulus, stress-strain and creep are actual material values multiplied by ratio of outer strand area to total area.

Note: Final modulus, stress-strain and creep are actual material values multiplied by ratio of core strand area to total area.

Bimetallic Conductor Model..

Aluminum has a larger thermal expansion coefficient than steel. If Aluminum is used as the outer material over a steel core there is a temperature transition point at which the aluminum is no longer under tension.

Select the behavior you want for temperatures above the transition point

Use behavior from Criteria/Bimetallic Conductor Model

Aluminum does not take compression at high temperature (Bird Cage)

Aluminum can go into compression at high temperature

$\frac{V_{Outer} \sigma_{Outer}}{A} = \frac{V_{Inner} \sigma_{Inner}}{A}$

$\frac{V_{Outer} \sigma_{Outer}}{A} = \frac{V_{Inner} \sigma_{Inner}}{A}$

$\sigma = \text{total cross section area of outer strands}$

$A = \text{total cross section area of entire conductor (outer + inner strands)}$

Maximum initial compressive stress: (MPa)

Thermal Rating Properties

Resistance at two different temperatures

Resistance (Ohm/km): 0.0427503 at (deg C) 25

Resistance (Ohm/km): 0.0520088 at (deg C) 75

Emissivity coefficient: 0.5

Solar absorption coefficient: 0.5

Outer strands heat capacity (Watt-s/m-deg C): 1812.7

Core heat capacity (Watt-s/m-deg C): 323.091

Generate Coefficients for outer strands from points on stress-strain or creep curves

Graph Cable Properties

Generate Coefficients for core strands from points on stress-strain or creep curves

Composite cable properties

OK Cancel

Figure A 8: PLS-CADD conductor file for Martin ACSS conductor in TW form

Appendix B

Structure Data Editor

Structure file name: c:\users\public\documents\pls\plc_518d 4bear tem:180

Description: 518 D / 1 arm

Height (ground to top of structure) (m): 25.65

Embedded length (for report purposes only) (m):

Lowest wire attachment point height above ground (m): 18.00

Set #	Phase #	Dead End Set	Set Description	Insulator Type	Insul. Weight (N)	Insul. Wind Area (cm ²)	Insul. Length (m)	Attach. Trans. Offset (m)	Attach. Dist. Below Top (m)	Attach. Longit. Offset (m)	Min. Req. Vertical Load (uplift) (N)	Allowable Suspension Swing Angles and 2-Parc Load Angles In,max for 4 condition: (deg)	Insul. Weight Side 2 (N)	Insul. Wind Area Side 2 (cm ²)	Insul. Length Side 2 (m)	Attach. Trans. Offset Side 2 (m)	Attach. Dist. below Top Side 2 (m)
1	1	1 Yes	E1	Clamp	NA	NA	NA	-13.20			No Uplift	NA	NA	NA	NA	NA	NA
2	2	1 Yes	E1	Clamp	NA	NA	NA	13.20			No Uplift	NA	NA	NA	NA	NA	NA
3	3	1 Yes	C1	Strain	520.00	2860.00	4.52	-14.55	7.65		No Uplift	NA	NA	NA	NA	NA	NA
4	3	2 NA	NA	Strain	520.00	2860.00	4.52		7.65		No Uplift	NA	NA	NA	NA	NA	NA
5	3	3 NA	NA	Strain	520.00	2860.00	4.52	11.10	7.65		No Uplift	NA	NA	NA	NA	NA	NA
6			NA	NA	NA	NA	NA	NA	NA	NA	NA	NA	NA	NA	NA	NA	NA
7			NA	NA	NA	NA	NA	NA	NA	NA	NA	NA	NA	NA	NA	NA	NA
8			NA	NA	NA	NA	NA	NA	NA	NA	NA	NA	NA	NA	NA	NA	NA
9			NA	NA	NA	NA	NA	NA	NA	NA	NA	NA	NA	NA	NA	NA	NA
10			NA	NA	NA	NA	NA	NA	NA	NA	NA	NA	NA	NA	NA	NA	NA
11			NA	NA	NA	NA	NA	NA	NA	NA	NA	NA	NA	NA	NA	NA	NA
12			NA	NA	NA	NA	NA	NA	NA	NA	NA	NA	NA	NA	NA	NA	NA
13			NA	NA	NA	NA	NA	NA	NA	NA	NA	NA	NA	NA	NA	NA	NA
14			NA	NA	NA	NA	NA	NA	NA	NA	NA	NA	NA	NA	NA	NA	NA
15			NA	NA	NA	NA	NA	NA	NA	NA	NA	NA	NA	NA	NA	NA	NA
16			NA	NA	NA	NA	NA	NA	NA	NA	NA	NA	NA	NA	NA	NA	NA
17			NA	NA	NA	NA	NA	NA	NA	NA	NA	NA	NA	NA	NA	NA	NA
18			NA	NA	NA	NA	NA	NA	NA	NA	NA	NA	NA	NA	NA	NA	NA
19			NA	NA	NA	NA	NA	NA	NA	NA	NA	NA	NA	NA	NA	NA	NA
20			NA	NA	NA	NA	NA	NA	NA	NA	NA	NA	NA	NA	NA	NA	NA

Struct. Strength Material Multiple Save Save As OK Cancel

Figure B 1: PLS-CADD structure file modelling 518 D structure

Appendices: Appendix B

Structure Data Editor

Structure file name: c:\user\public\documents\pl\pl_cadd_1520b_45w240

Description: 520 C 1500mm structure

Height (ground to top of structure): (m) 30.14

Embedded length (for report purposes only): (m)

Lowest wire attachment point height above ground: (m) 24.00

	Sec #	Phase #	Dead End Set	Set Description	Insulator Type	Insul. Weight (N)	Insul. Wind Area (cm ²)	Insul. Length (m)	Attach. Trans. Offset (m)	Attach. Dist. Below Top (m)	Attach. Longit. Offset (m)	Min. Req. Vertical Load (uplift) (N)	Allowable Suspension Swing Angles and 2-Part Load Angles min,max for 4 conditions (deg)	Insul. Weight Side 1 (N)	Insul. Wind Area Side 1 (cm ²)	Insul. Length Side 1 (m)	Attach. Trans. Offset Side 1 (m)	Attach. Dist. Below Top Side 1 (m)	Attach. Longit. Offset Side 1 (m)	
1	1	1	Yes	E1	Clamp	NA	NA	NA	-7.13	0.23		No Uplift	NA	NA	NA	NA	NA	NA	NA	
2	2	1	No	E1	Clamp	NA	NA	NA	7.13	0.23		No Uplift	NA	NA	NA	NA	NA	NA	NA	
3	3	1	No	C1	2-Part	520.00	2860.00	4.52	-11.70	2.95		No Uplift	-45, 45 -47, 47 -53, 53 -9	520.00	2860.00	4.52	-5.30	2.95		
4	3	2	NA	NA	2-Part	520.00	2860.00	4.52	-3.20	2.95		No Uplift	-45, 45 -47, 47 -53, 53 -9	520.00	2860.00	4.52	3.20	2.95		
5	3	3	NA	NA	2-Part	520.00	2860.00	4.52	5.30	2.95		No Uplift	-45, 45 -47, 47 -53, 53 -9	520.00	2860.00	4.52	11.70	2.95		
6			NA	NA	NA	NA	NA	NA	NA	NA	NA	NA	NA	NA	NA	NA	NA	NA	NA	NA
7			NA	NA	NA	NA	NA	NA	NA	NA	NA	NA	NA	NA	NA	NA	NA	NA	NA	NA
8			NA	NA	NA	NA	NA	NA	NA	NA	NA	NA	NA	NA	NA	NA	NA	NA	NA	NA
9			NA	NA	NA	NA	NA	NA	NA	NA	NA	NA	NA	NA	NA	NA	NA	NA	NA	NA
10			NA	NA	NA	NA	NA	NA	NA	NA	NA	NA	NA	NA	NA	NA	NA	NA	NA	NA
11			NA	NA	NA	NA	NA	NA	NA	NA	NA	NA	NA	NA	NA	NA	NA	NA	NA	NA
12			NA	NA	NA	NA	NA	NA	NA	NA	NA	NA	NA	NA	NA	NA	NA	NA	NA	NA
13			NA	NA	NA	NA	NA	NA	NA	NA	NA	NA	NA	NA	NA	NA	NA	NA	NA	NA
14			NA	NA	NA	NA	NA	NA	NA	NA	NA	NA	NA	NA	NA	NA	NA	NA	NA	NA
15			NA	NA	NA	NA	NA	NA	NA	NA	NA	NA	NA	NA	NA	NA	NA	NA	NA	NA
16			NA	NA	NA	NA	NA	NA	NA	NA	NA	NA	NA	NA	NA	NA	NA	NA	NA	NA
17			NA	NA	NA	NA	NA	NA	NA	NA	NA	NA	NA	NA	NA	NA	NA	NA	NA	NA
18			NA	NA	NA	NA	NA	NA	NA	NA	NA	NA	NA	NA	NA	NA	NA	NA	NA	NA
19			NA	NA	NA	NA	NA	NA	NA	NA	NA	NA	NA	NA	NA	NA	NA	NA	NA	NA
20			NA	NA	NA	NA	NA	NA	NA	NA	NA	NA	NA	NA	NA	NA	NA	NA	NA	NA

Struct Strength Material Multiple Save Save As OK Cancel

Figure B 2: PLS-CADD structure file modelling 520 B structures

Structure Data Editor

Structure file name: d:\documents and settings\user11\my docu...1518c_45w300

Description: 518c 45deg 4x7m

Height (ground to top of structure): (m) 36.10

Embedded length (for report purposes only): (m)

Lowest wire attachment point height above ground: (m) 20.00

	Set #	Phase #	Dead End Set	Set Description	Insulator Type	Insul. Weight (N)	Insul. Wind Area (cm ²)	Insul. Length (m)	Attach. Trans. Offset (m)	Attach. Dist. Below Top (m)	Attach. Longit. Offset (m)	Min. Req. Vertical Load (uplift) (N)	Allowable Suspension Swing Angles and 2-Part Load Angles min,max for 4 conditions (deg)
1	1	1	Yes	E1	Clamp	NA	NA	NA	-11.16			No Limit	NA
2	2	1	Yes	E1	Clamp	NA	NA	NA	11.16			No Limit	NA
3	3	1	Yes	C1	Strain	1000.00	12000.00	4.90	-12.80	6.10		No Limit	NA
4	3	2	NA	NA	Strain	1000.00	12000.00	4.90		6.10		No Limit	NA
5	3	3	NA	NA	Strain	1000.00	12000.00	4.90	10.50	6.10		No Limit	NA
6			NA	NA	NA	NA	NA	NA	NA	NA	NA	NA	NA
7			NA	NA	NA	NA	NA	NA	NA	NA	NA	NA	NA
8			NA	NA	NA	NA	NA	NA	NA	NA	NA	NA	NA
9			NA	NA	NA	NA	NA	NA	NA	NA	NA	NA	NA
10			NA	NA	NA	NA	NA	NA	NA	NA	NA	NA	NA
11			NA	NA	NA	NA	NA	NA	NA	NA	NA	NA	NA
12			NA	NA	NA	NA	NA	NA	NA	NA	NA	NA	NA
13			NA	NA	NA	NA	NA	NA	NA	NA	NA	NA	NA
14			NA	NA	NA	NA	NA	NA	NA	NA	NA	NA	NA
15			NA	NA	NA	NA	NA	NA	NA	NA	NA	NA	NA

Struct Strength Material Multiple Save Save As OK Cancel

Figure B 3: PLS-CADD structure file modelling 518 C structures

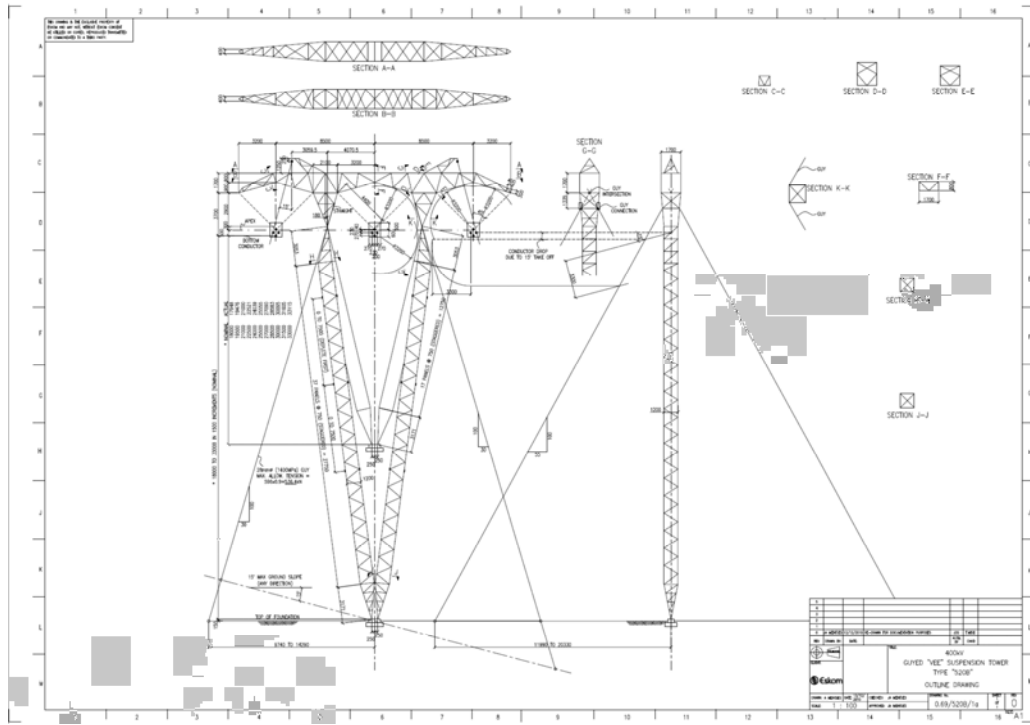


Figure B 4: Outline drawing for 520 B structure

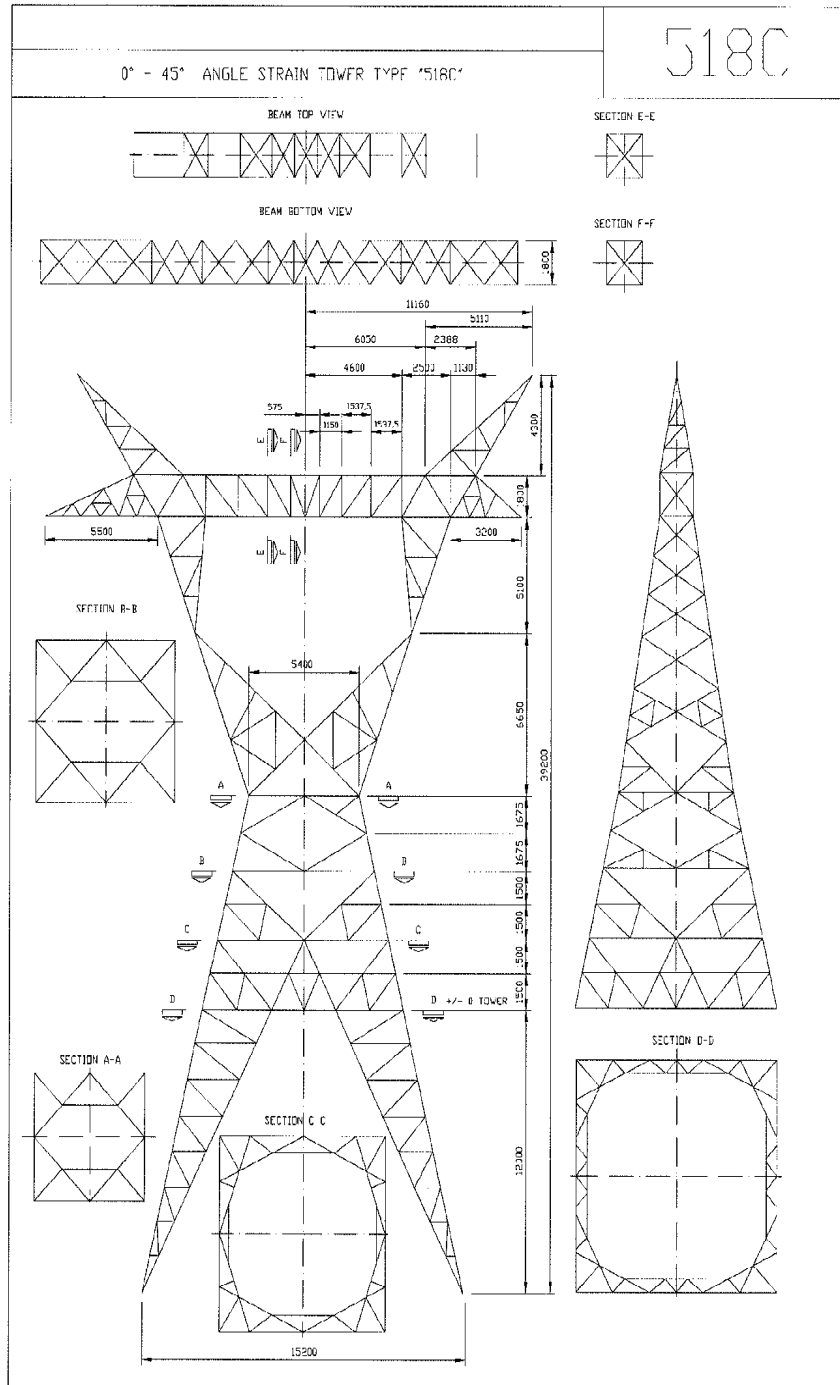


Figure B 5: Outline drawing for 518 C structure

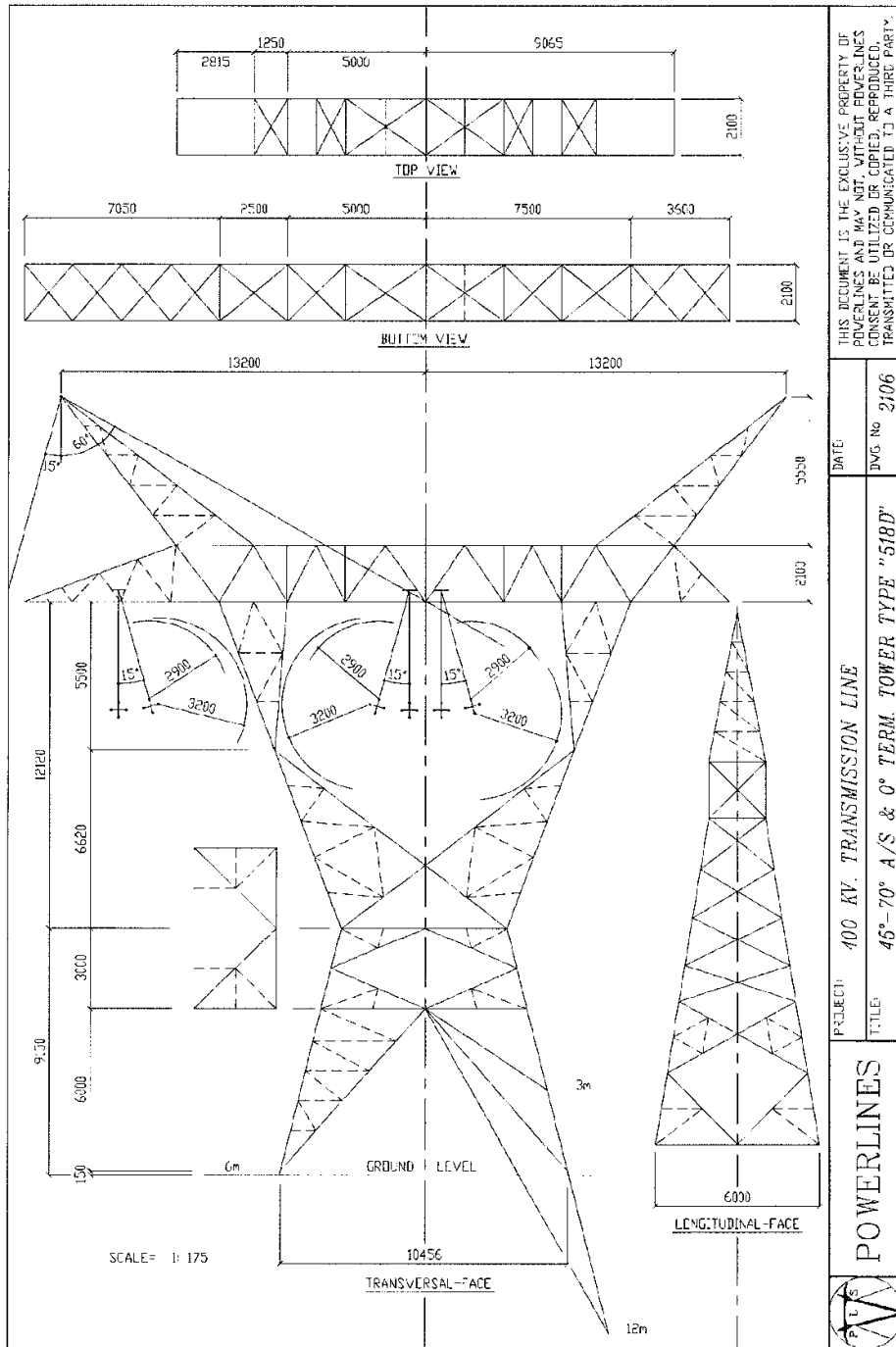


Figure B 6: Outline drawing for 518 D structure

Appendix C

Table C-1: Ampacity of IEEE and CIGRÉ for Martin ACSR conductor in TW shape

Martin ACSR TW	Tc = 70 (°C)			Tc = 80 (°C)			Tc = 90 (°C)			Tc = 100 (°C)		
	IEEE		CIGRÉ	IEEE		CIGRÉ	IEEE		CIGRÉ	IEEE		CIGRÉ
	Clear	Industrial		Clear	Industrial		Clear	Industrial		Clear	Industrial	
Qs (Watts/m)	19.57	15.89	18.86	19.57	15.89	18.86	19.57	15.89	18.86	19.57	15.89	18.86
Qc (Watts/m)	18.78	18.78	20.47	26.7	26.7	29.2	35.03	35.03	38.44	43.67	43.67	48.09
Qr (Watts/m)	12.48	12.48	12.48	17.45	17.45	17.45	22.85	22.85	22.85	28.71	28.71	28.71
Current (A)	481	552	528	687	736	730	844	884	888	976	1010	1010

Appendices: Appendix C

Table C-2: Ampacity of IEEE and CIGRÉ for Martin ACSR conductor in RW shape

Martin ACSR RW	Tc = 70 (°C)			Tc = 80 (°C)			Tc = 90 (°C)			Tc = 100 (°C)		
	IEEE		CIGRÉ	IEEE		CIGRÉ	IEEE		CIGRÉ	IEEE		CIGRÉ
	Clear	Industrial		Clear	Industrial		Clear	Industrial		Clear	Industrial	
Qs (Watts/m)	21.27	17.27	20.49	21.27	17.27	20.49	21.27	17.27	20.49	21.27	17.27	20.49
Qc (Watts/m)	42.2	42.2	43.8	56.24	56.24	58.44	70.27	70.27	73.12	84.29	84.29	87.83
Qr (Watts/m)	13.68	13.68	13.68	19.11	19.11	19.11	25.03	25.03	25.03	31.45	31.45	31.45
Current (A)	821	867	848	1010	1047	1038	1164	1195	1193	1296	1323	1326

Table C-3: Ampacity of IEEE and CIGRÉ for Tern ACSR conductor in RW

Tern ACSR RW	Tc = 70 (°C)			Tc = 80 (°C)			Tc = 90 (°C)			Tc = 100 (°C)		
	IEEE		CIGRÉ	IEEE		CIGRÉ	IEEE		CIGRÉ	IEEE		CIGRÉ
	Clear	Industrial		Clear	Industrial		Clear	Industrial		Clear	Industrial	
Qs (Watts/m)	15.88	12.89	15.3	15.88	12.89	15.3	15.88	12.89	15.3	15.88	12.89	15.3
Qc (Watts/m)	36.37	36.37	38.17	48.47	48.47	50.93	60.57	60.57	63.71	72.66	72.66	76.53
Qr (Watts/m)	10.21	10.21	10.21	14.27	14.27	14.27	18.68	18.68	18.68	23.48	23.48	23.48
Current (A)	597	625	619	726	749	749	831	851	855	922	939	947

Table C-4: Ampacity of IEEE and CIGRÉ for Tern ACSR conductor in TW

Tern ACSR TW	Tc = 70 (°C)			Tc = 80 (°C)			Tc = 90 (°C)			Tc = 100 (°C)		
	IEEE		CIGRÉ	IEEE		CIGRÉ	IEEE		CIGRÉ	IEEE		CIGRÉ
	Clear	Industrial		Clear	Industrial		Clear	Industrial		Clear	Industrial	
Qs (Watts/m)	14.34	11.64	13.81	14.34	11.64	13.81	14.34	11.64	13.81	14.34	11.64	13.81
Qc (Watts/m)	34.54	34.54	36.38	46.03	46.03	48.54	57.52	57.52	60.73	69	69	72.94
Qr (Watts/m)	9.22	9.22	9.22	12.88	12.88	12.88	16.87	16.87	16.87	21.2	21.2	21.2
Current (A)	589	615	612	713	734	737	815	833	840	902	918	928